SKB

TECHNICAL REPORT 85-12

Hydrogeological investigations and tracer tests in a well-defined rock mass in a The Stripa mine

Peter Andersson
Carl-Erik Klockars
Swedish Geological Company

Division of Engineering Geology
Uppsala 1985-11-29

SVENSK KÄRNBRÄNSLEHANTERING AB
SWEDISH NUCLEAR FUEL AND WASTE MANAGEMENT CO

BOX 5864 S-102 48 STOCKHOLM
TEL 08-665 28 00 TELEX 13108-SKB

HYDROGEOLOGICAL INVESTIGATIONS AND TRACER TESTS IN A WELL-DEFINED ROCK MASS IN THE STRIPA MINE

Peter Andersson
Carl-Erik Klockars

Swedish Geological Company
Division of Engineering Geology
Uppsala 1985-11-29

A list of other reports published in this series during 1985 is attached at the end of this report. Information on technical reports from 1977-1978 (TR 121) 1979 (TR 79-28), 1980 (TR 80-26), 1981 (TR 81-17), 1982 (TR 82-28), 1983 (TR 83-77) and 1984 (TR 85-01) is available through SKB.

SWEDISH GEOLOGICAL COMPANY
Division of Engineering Geology
Client: SKB

REPORT
Date: 1985-11-29
ID-no: IRAP 85255

HYDROGEOLOGICAL INVESTIGATIONS AND TRACER TESTS IN A WELL-DEFINED ROCK MASS IN THE STRIPA MINE

Peter Andersson
Carl-Erik Klockars

SGAB, Uppsala

ABSTRACT

This report presents the results from hydraulic tests and tracer test in a well-defined, fractured, but low conductive granite in the Stripa mine. The purpose has been to study the properties of the rock and the fractures regarding hydraulic conductivity (K) and tracer transport.

The K-value of the rock has been determined by hydraulic single-hole tests. The heterogeneity of the rock has been studied by hydraulic cross-hole tests and the transport mechanisms and fracture properties by non-sorbing tracer test. The test configuration is cylindrical with injection in the centre hole and detection in 8 peripheral holes evenly distributed on the mantle area of a cylinder, radius 1.5 m.

The result from the single-hole tests in 1 m sections show a K-value between 1 E-9 and 7 E-12 m/s. The cross-hole tests indicate that the rock cannot be treated as a homogeneous, anisotropic, porous medium in the scale of this investigation. However, the method is a valuable help in identifying flow paths. The tracer test indicates that 3 % of the total number of fractures are conducting water and that channeling occurs within the fracture planes. From the tracer test and the hydraulic tests, hydraulic fracture conductivity, flow porosity and longitudinal dispersion have been determined for different flow paths within the same distance from the injection hole.

CONTENTS

SUMMARY

The purpose of this investigation has been to study the properties of the rock mass and the fractures regarding hydraulic conductivity and tracer transport in a well-defined, fractured, but low conductive rock mass in the Stripa mine. The hydraulic properties of the rock mass have been determined by hydraulic single-hole tests. The heterogenity of the rock has been studied by hydraulic cross-hole tests and the transport mechanisms and fracture properties by a non-sorbing tracer test.

The results and conclusions of the tests can be summarized as follows:

- The hydraulic conductivity from single-hole tests (1 m sections) varies between 1 E-9 - 7 E-12 m/s.

- The cross-hole tests indicate that the rock mass cannot be treated as a homogeneous, anisotropic, porous medium in the scale of this investigation.

- Directional hydraulic conductivities have been calculated from cross-hole tests (0.5 m sections) ranging between 7.1 E-10 - 4.8 E-11 m/s.

- The cross-hole tests have proved to be of valuable help in indicating possible flow paths or channels.

- The tracer test indicates that flow occurs within a few well connected fractures and that the channeling within the fracture planes is strong and the flow geometry is affected by small changes in the hydraulic head distribution.

- The water conducting fractures are on an average 3 % of the total number of fractures.

- Instead of fracture width, the hydraulic fracture conductivity K_e, has been used to express the hydraulic properties of a fracture. K_e has been determined in two different ways, with the residence time, t_o, and with the flow rate to the observation holes, q, as basic variable with both radial and linear flow assumptions. The mean values are 2.9 E-7 m/s and 1.1 E-5 m/s, respectively with the radial flow assumption. The linear flow assumption gives K_e^t = 1.7 E-7 m/s and K_e^q = 4.8 E-6 m/s.

- The ratio K_e^q/K_e^t was on an average 50 with the radial flow assumption and was found to increase with increasing residence time. Available data indicate a linear increase with the logarithm of the residence time. The explanation for this may be that K_e^t represents the volume of the fracture while K_e^q represents the narrowest paths of the fracture. The diffusion may also affect K_e^q/K_e^t in a similar way.

- The flow porosity has been calculated as a volumetric ratio and as a conductivity ratio. The calculated values are 6.7 E-5 and 3.8 E-4 respectively.

- The longitudinal dispersion within individual flow paths is very low. The dimensionless dispersion parameter $n = D/vx < 0.01$.

- The longitudinal dispersion parameter for the total flow to the sampling section, i.e. the macrodispersion, ranges between n = 0.03 - 0.08.

- The active area of a fracture plane regarding the flow, defined as the area of a fracture where transport occurs, has been estimated to 50 % of the total area of the fracture plane by probability calculations.

1. BACKGROUND AND PURPOSE

The movement of the groundwater in crystalline bedrock is chiefly dependent upon existing fractures. Knowledge of the transport mechanisms and the diluting factors for sorbing and non-sorbing substances is a very important part of the safety analysis of the problems associated with the storage of nuclear waste in the Precambrian bedrock.

Within the KBS/SKB program, tracers have previously been used for studies of the groundwater movement by Landström et al (1978, 1983) and Gustafsson, Klockars (1981, 1984). These tests have been carried out in highly conductive (K = E-7 - E-6 m/s) fracture zones and have illuminated transport mechanisms within distances of 10-30 meters. Transport within shorter distances in low conductive rock will most probably take place in individual fractures. In this investigation, performed in the Stripa mine, hydraulic tests and tracer tests have been carried out in a well defined, low conductive (K = E-11 - E-10 m/s) rock mass.

The purpose of this investigation has been to study the properties of the rock mass and fractures regarding hydraulic conductivity and tracer transport. The studies can be summarized as follows:

- Comparison of the results from different hydraulic tests to the tracer test
- Studies of the heterogeneity of the rock mass, including channeling
- Determinations of flow porosity and dispersivity parameters in low conductive rock
- Using the result from the non-sorbing tracer test to predict and design tests with sorbing tracers
- Development of techniques for performing tracer tests

2. HYDRAULIC TESTS

2.1 Single-hole tests

Single-hole tests are especially attractive when a large number of measurements must be performed e.g. in determining the hydraulic conductivity profile of boreholes. The volume of rock, sampled by a single-hole test, is often limited to the immediate vicinity of the borehole. Nevertheless, single-hole tests are valuable, and often necessary for making preliminary studies of a field site and to establish a data base upon which further hydraulic tests and tracer tests can be designed.

In this investigation, transient single-hole injection tests with constant excess pressure have been performed. The method of interpreting these tests in the transient stage is based on the assumption that the rock can be treated as a homogeneous, isotropic, closed aquifer, for which the governing equation according to Walton (1970) is:

$$\frac{\partial^2 h}{\partial r^2} + \frac{1}{r}\frac{\partial h}{\partial r} = \frac{S}{T}\frac{\partial h}{\partial t} \qquad (r > r_w) \qquad (1)$$

where h = hydraulic head at the distance r (m)
r = distance from injection hole (m)
r_w = radius of injection hole (m) t = time (s)
S = storage coefficient of the aquifer
T = transmissivity (m^2/s)

The boundary conditions at constant pressure H_o can be written as:

$$\lim_{r \to \infty} h = 0 \qquad (2)$$

$$h(r, t<0) = 0 \qquad (3)$$

The solution to equation (1) can, according to Uraiet and Rag-

havan (1980) be approximated by:

$$K = \frac{0.183}{H_o \cdot L \cdot \Delta(1/Q(t))} \qquad (4)$$

where K = hydraulic conductivity (m/s)

H_o = excess pressure in the injection section (m)

L_o = length of injection section (m)

$\Delta(1/Q(t))$ = change in $1/Q(t)$ per decade of time (s/m^3)

t_D = dimensionless time defined by (5)

$$t_D = \frac{K \cdot t}{r_w^2 \cdot S_s} \qquad (5)$$

where S_s = specific storage (m^{-1})

The data are plotted in a semilogarithmic diagram with $1/Q(t)$ as a function of log t, K is evaluated from the slope of the straight line according to eq (4).

2.2 Cross-hole tests

The greatest advantage of cross-hole tests, in general, is that a larger volume of the rock mass is tested and a more well-defined test geometry is achived than in the case of single-hole tests. In this study a new field method, proposed by Hsieh et al (1983), for determining the three-dimensional anisotropic hydraulic conductivity of a fractured rock, has been tested. This approach attempts to determine the hydraulic conductivity tensor from two non-parallel or three parallel boreholes without knowing the directions of the principal hydraulic conductivities prior to the test. In addition to hydraulic conductivity, the specific storage of the rock mass can also be determined.

The test procedure consists of injecting water of a constant flow rate into a packed-off section in one borehole and monitoring the responding pressure increase in packed-off sections

within one or more neighbouring boreholes.

The fractured rock mass is assumed to be a homogeneous, anisotropic porous medium. The governing equation of fluid flow is:

$$\underline{\nabla}_o (\underline{K}\, \underline{\nabla} h) = S_s \frac{\partial h}{\partial t} \qquad (6)$$

h = hydraulic head (m)
$\underline{K}$ = hydraulic conductivity tensor (m/s)
S_s = specific storage (m^{-1})
$\underline{\nabla}_o$ = divergence operator
$\underline{\nabla}$ = gradient operator

If the initial head distribution is uniform and the flow domain is of infinite extent, the initial and boundary conditions are, respectively,

$$h(\underline{x},t) = h_o \text{ at } t = 0 \qquad (7a)$$
$$h(\underline{x},t) = h_o \text{ as } x_i \to \infty \qquad (7b)$$

The solution for a continuous point source injecting at a constant volumetric rate Q at the origin of the x_1, x_2, x_3 coordinate system is, according to Hsieh et al (1983):

$$\Delta h = \frac{Q}{4\pi \cdot R} \left(\frac{K_d(\underline{n})}{D}\right)^{1/2} \cdot \operatorname{erfc}\left(\frac{R^2 \cdot S_s}{4K_d(\underline{n}) \cdot t}\right)^{1/2} \qquad (8)$$

where R = distance between injection and monitoring sections (m)
$K_d(\underline{n})$ = directional hydraulic conductivity (m/s)
D = determinant of $\underline{K}$ (m^3/s^3)
erfc = complementary error function

The directional hydraulic conductivity is defined as:

$$K_d(\underline{n}) = -|\underline{q}| / (\underline{n}^T \underline{\nabla} h) \qquad (9)$$

where $\underline{q}$ = specific discharge (m^3/s)
∇h = hydraulic gradient (m/m)
$\underline{n}$ = unit vector in the direction of $\underline{q}$
$\underline{n}^T$ = transpose unit vector

Darcy's law together with (9) gives the expression

$$K_d(\underline{n}) = 1/(\underline{n}^T \underline{K}^{-1} \cdot \underline{n}) \qquad (10)$$

Equation (10) represents an ellipsoid defined by the radius vector $\sqrt{K_d(\underline{n})}.\underline{n}$. The semi-axes of the ellipsoid are the square roots of the principal hydraulic conductivities and point in the principal directions of $\underline{K}$, see figure 1. Equation (8) can also be written in dimensionless form as

$$\Delta h_{PD} = \text{erfc}\ (1/4t_D)^{1/2} \qquad (11)$$

where h_{PD} and t_D are defined by

$$h_{PD} = (4\pi \cdot R \cdot \Delta h/Q) \cdot (D/K_d(\underline{n}))^{1/2} \qquad (12)$$

$$t_D = K_d(\underline{n}) \cdot t/R^2 \cdot S_s \qquad (13)$$

Let $\underline{e}$ be the unit vector pointing from the point source at the origin of the cartesian axes, x_i to a monitoring section represented by a point at $R_j\underline{e}_j$ (figure 2). The test results can now be analysed by curve-matching if $R_j\ h_j/Q$ versus t/R^2 is plotted on log-log paper and compared with the type curve prepared from equation (11). From the curve-matching and equations (12) and (13), the directional diffusivity $K_d(\underline{e}_j)/S_s$ and the quantity $D/K_d(\underline{e}_j)$ can be computed. Also D/S_s can be obtained from the product of the above two quantities.

The validity of treating the fractured rock as a homogeneous anisotropic, porous medium may be examined on the basis of the

following criteria:

1) The data should fit the type curve
2) The computed values of D/S_s from all observation points should be approximately the same
3) A plot of $(K_d(e_j)/S_s)^{1/2}$ versus the directions $\underline{e}_j$ should outline an ellipsoid as in figure 1

To determine the six components of the hydraulic conductivity tensor, at least six observation points are needed, not more than two observation points along a line or more than three in a plane.

Replacing $\underline{n}$ in equation (10) with $\underline{e}_j$, multiplying with S_s and expanding, the following equation can be written for each observation point j:

$$e_{j1}^2 U_{11} + e_{j2}^2 U_{22} + e_{j3}^2 U_{33} + 2e_{j1} e_{j2} U_{12} + \\ + 2e_{j2} e_{j3} U_{23} + 2e_{j1} e_{j3} U_{13} = S_s/K_d(\underline{e}_j) \qquad (14)$$

where $\underline{U}$ is defined by

$$\underline{U} = S_s / K \qquad (15)$$

By solving an equation system of six equations where e_{j1}, e_{j2}, e_{j3} are known from the location of the points and $S_s/K_d(\underline{e}_j)$ is determined from the curve matching, the inverse diffusivity tensor $\underline{U}$ can be obtained. Inverting $\underline{U}$ gives the diffusivity tensor $\underline{K}/S_s$ and by computing the quantity D/S_s^3, which is the determinant of $\underline{U}^{-1}$, S_s can be obtained from:

$$S_s = \left[(\overline{D/S_s}) \; / \; (D/S_s^3) \right]^{1/2} \qquad (16)$$

where $(\overline{D/S_s})$ is the average of the D/S_s values for all the tests. Finally, the components of the hydraulic conductivity tensor $\underline{K}$ can be calculated by multiplying $\underline{K}/S_s$ by S_s.

The validity of representing the injection interval and monitoring intervals as points has been treated theoretically by Hsieh et al (1985). They showed that an injection interval of length L may be represented by a point whenever

$$\alpha_1 = (2\ R/L) \cdot (K_d(\underline{e}_1) / K_d(\underline{e}))^{1/2} \geq 5.0 \qquad (17)$$

An observation interval of length B may be represented by a point whenever

$$\beta_1 = (2\ R/B) \cdot (K_d(\underline{e}_b) / K_d(\underline{e}))^{1/2} \geq 5.0 \qquad (18)$$

$\underline{e}_1$ and $\underline{e}_b$ are unit vectors parallel to the injection and monitoring intervals and $\underline{e}$ is a unit vector pointing from the center of the injection interval to the center of the monitoring interval.

3. TRACER TEST

3.1 Flow and residence time

The test site can schematically be described as a cylinder. A tracer solution with concentration C_o is injected in the centre of the cylinder. The tracer is detected in 8 peripheral holes evenly distributed on the mantle area of the cylinder. Assuming that all of the moving water in the fractures is exchanged by the tracer solution and that the inflow to the detection holes equals the outflow i.e. constant volume, and that complete mixing is established. The equation of continuity can then be written:

$$\frac{dc}{dt} = \left(C_o - C(t) \right) \cdot \frac{Q}{V} \qquad (19)$$

where $C(t)$ = concentration of tracer in the sampling section at time t
Q = tracer flow (m^3/s)
V = volume of the sampling section (m^3)

The solution to eq (19) with the boundary condition

$$C(t) = 0 \quad \text{at } t = 0 \qquad (20)$$

can be written

$$C(t) = C_o \left(1 - e^{-t/T_o}\right) \qquad (21)$$

where $$T_o = V / Q \qquad (22)$$

Equation (21) is illustrated in figure 3 and can for low values of t/T_o, be approximated by a straight line. The straight line approximation deviates less than 1 % from the theoretical value after t = 1000 h.
Assuming constant volume V and $C_o >> C(t)$, the tracer flow Q can be calculated from the slope of the straight line:

$$Q = \frac{\Delta C}{\Delta t} \cdot \frac{V}{C_o} \qquad (23)$$

From the breakthrough curve, several flow channels can be identified as changes in the slope of the straight line as shown in figure 4. An increase in the slope means an increase in the flow to the hole i.e. an additional flow channel is involved in the tracer transport to the observation hole. The flow rates of the additional flow channels are calculated as shown in figure 4. The mean residence time t_o of a flow channel is defined as the time where the slope is changed in the breakthrough curve. This is correct as long as the dispersion is negligible.

3.2 Hydraulic fracture conductivity

The most common way to express the hydraulic porperties of fractures is by means of some kind of fracture width. However, the term fracture width is not an actual geometric property as the fracture width may vary considerably across a fracture plane. In some parts the fractures can be entirely closed while in others big "lakes" can occur. This is supported by tracer tests performed by Gustafsson and Klockars (1981) and Albelin et al (1985) which have shown that the transport of water occurs within concentrated flow paths (channels) in a fracture plane. Thus, the fracture width describing some theoretical equivalent, plane-parallel fracture width, is of less use. In this investigation, the term hydraulic fracture conductivity, K_e, has been used instead. K_e can be determined in different ways depending on the assumptions made. The flow to the observation holes can either be approximated by a diverging radial flow or by a linear flow assumption.

Applying Darcy's law to an injection of water to a vertical borehole in a radial flow geometry (figure 5):

$$v = - K_e \frac{\partial p}{\partial r} \qquad (24)$$

v	= mean velocity of water	(m/s)
K_e	= hydraulic fracture conductivity	(m/s)
$\partial p/\partial r$	= pressure gradient	(m/m)
r	= distance from injection hole	(m)

The flow, Q, from a borehole into a fracture with fracture width e, can be written:

$$Q = 2\pi r \cdot e \quad v \tag{25}$$

Combination of eq (24) and eq (25) and integration gives:

$$K_e = \frac{Q \cdot \ln(r/r_w)}{2\pi \cdot e \cdot \Delta h} \tag{26}$$

where r_w = radius of injection hole (m)
Δh = difference in hydraulic head between injection and observation hole (m)

There are two ways of eliminating the fracture width from equation (26), with the residence time, t_o, or with the flow rate, q, as basic variable. In the first case, the flow in a fracture can be written:

$$Q = \frac{\pi \cdot (r^2 - r_w^2) \cdot e}{t_o} \tag{27}$$

Substitution in eq (26) gives:

$$K_e{}^t = \frac{(r^2 - r_w^2) \cdot \ln (r/r_w)}{2 \cdot t_o \cdot \Delta h} \tag{28}$$

Equation (28) represents the hydraulic fracture conductivity calculated with the residence time, t_o, as basic variable. The fracture width in equation (27) is a volumetric fracture width which implies that $K_e{}^t$ represents the kinematic volume of a fracture.

According to Snow (1968), the hydraulic conductivity for laminar flow between two parallel plates, can be written:

$$K_e = \frac{e^2 \cdot g}{12\ \nu} \tag{29}$$

where g = acceleration due to gravity (m/s^2)
ν = kinematic viscosity (m^2/s)

Combination of equation (26) and (29) give the hydraulic fracture conductivity as a function of geometry and flow rate:

$$K_e = \left[\frac{Q \cdot \ln(r/r_w) \cdot \sqrt{g}}{2\pi \cdot \Delta h \cdot \sqrt{12\nu}} \right]^{2/3} \qquad (30)$$

However, The flow, q, to each observation hole at the distance r from the injection hole can be homogeneously distributed over the active radius, l, of the observation hole:

$$q = \frac{l}{2\pi \cdot r} \cdot Q \qquad (31)$$

Substitution of eq (31) into eq (30) gives:

$$K_e^q = \left[\frac{q \cdot r \cdot \ln(r/r_w) \cdot \sqrt{g}}{l \cdot \Delta h \cdot \sqrt{12\nu}} \right]^{2/3} \qquad (32)$$

Equation (32) represents the hydraulic fracture conductivity calculated with the flow rate, q, as basic variable. Along a flow path in a fracture of variable width, the flow rate will be determined by the narrowest passage and thus the fracture width in eq (29) will represent the smallest width along the flow path. Consequently, the fracture width in eq (29) will be equal to the volumetric fracture width only in smooth parallel channels. Thus, K_e^q and K_e^t represent different ways of describing the same hydraulic property of fractures.

K_e^q and K_e^t can also be calculated assuming linear flow conditions. Equation (28) then becomes:

$$K_e^t = \frac{L^2}{t_o \cdot \Delta h} \qquad (33)$$

where L = distance between injection and observation hole (m)

K_e^q can be linearized in the same way to:

$$K_e^q = \left[\frac{q \cdot L \cdot \sqrt{g}}{l \cdot \Delta h \cdot \sqrt{12\nu}} \right]^{2/3} \qquad (34)$$

3.3 Flow porosity

The porosity of a rock can, according to Norton and Knapp (1977) be represented by

$$\theta_T = \theta_k + \theta_d + \theta_r \qquad (35)$$

where θ_T = total porosity
θ_k = kinematic or flow porosity
θ_d = diffusion porosity
θ_r = residual porosity

The total porosity includes all fracture openings and pores within the rock mass, but when studying groundwater movements, the most interesting property is the volume of pore space involved in fluid transportation. This property is called the kinematic or flow porosity and in some cases the effective porosity.

There are also discontinuous fractures or fractures of such small width that the water cannot move under prevailing hydraulic conditions. These fractures, where the transport of aqueuos components is governed by diffusion, makes up the diffusion porosity. The last term, the residual porosity includes all remaining pore volumes and is more than 90 % of the total porosity according to Norton and Knapp (1977).

The flow porosity can be calculated as the ratio between the hydraulic fracture conductivity, K_e, and the conductivity of the rock mass K, providing Darcy´s law is valid and that the gradient is equally large over the rock mass and over the fracture.

$$\theta_{kk} = K / K_e \qquad (36)$$

Equation (36) implies that flow porosity is a directional property, varying in the same way as the hydraulic fracture conductivity in different directions. However, in this work, the directional dependency has been thoroughly described by the hydraulic fracture conductivity determinations (chapter 7.2)

and the flow porosity is here given as a mean value of all directions.

The flow porosity can also be calculated as a volumetric ratio between the volume of moving water within the rock mass, V_w, and the total volume of the rock mass, V_r.

$$\theta_{kv} = V_w / V_r \qquad (37)$$

The volume of water in the rock mass is calculated from:

$$V_w = Q_c \cdot t_o \qquad (38)$$

where Q_c = injection flow rate (m^3/s)
t_o = mean residence time of water (s)

3.4 Dispersion

A water-soluble substance that is transported with the groundwater will be spread in time and space. This spreading, dispersion, occurs both in the flow direction of the groundwater and perpendicular to the direction, is called dispersion. The dispersion is dependent upon two factors:

- o the velocity distribution in the medium
- o molecular diffusion

The portion of dispersion that is dependent upon the velocity distribution in the fracture system is termed mechanical dispersion and is given by the general dispersion equation for one-dimensional flow of non-reactive substances:

$$\frac{\partial C}{\partial t} = D_l \cdot \frac{\partial^2 C}{\partial x^2} - v \frac{\partial C}{\partial x} \qquad (39)$$

where C = concentration of the non-reactive substance in the groundwater
D_l = longitudinal dispersion coefficient (m^2/s)
v = average transport velocity of groundwater (m/s)
x = coordinate in flow direction (m)
t = time variable (s)

In the case of continuous injection with constant flow and tracer concentration C_o, equation (39) has the following solution for one-dimensional flow (Ogata and Banks, 1961):

$$\frac{C}{C_o} = \frac{1}{2}\left[\operatorname{erfc}\frac{1 - t/t_o}{2\sqrt{n \cdot t/t_o}} + e^{1/r} \cdot \operatorname{erfc}\frac{1 + t/t_o}{2\sqrt{n \cdot t/t_o}}\right] \quad (40)$$

where t_o = mean residence time of groundwater (s)
$n = D_l/v \cdot x$ = dispersion parameter (dim.less)
$1/n$ = Peclet's number

Equation (40) is valid only for purely mechanical dispersion where the dispersivity D/v can be assumed to be constant and molecular diffusion can be neglected (Zuber, 1974).

3.5 Channeling in low conductive rock

Fracture frequency in drillcores is usually badly correlated to hydraulic conductivity. This is particularly evident in low conductive crystalline rock at greater depths. One explanation can be that only a limited number of the fractures are open and continuous enough to be conducting water under prevailing gradient conditions.

Tracer tests make it possible to determine the number of fractures involved in the flow. Thus, the percentage of fractures carrying tracer can be determined if the total fracture frequency is known from drillcore logs or camera inspections of boreholes.

An attempt has been made to study the active area, regarding the flow, of a fracture plane. This active area is defined as the area of a fracture plane that is open and in which the

transport of groundwater is taking place. The probability of observing a tracer-carrying fracture is dependent upon the active area of the fracture. If the observation probability is p and n is the maximum number of tracer-carrying fractures, the number of observed tracer carrying fractures is binomially distributed:

$$Pr\,(z=x) = \binom{n}{x} \cdot p^{x}(1-p)^{n-x} \quad (x = 0,1, \ldots, n) \qquad (41)$$

where z = stochastic variable
$Pr\,(z=x)$ = The probability that the stochastic variable is equal to x
x = number of observed tracer carrying fractures

Assuming that the active area of a fracture is equal to the observation probability, an estimate of the active area can be made if, as in Stripa, the probability of observing x tracer-carrying fractures is known.

4. TEST SITE

4.1 General description

The SGAB tracer test drift is situated at the 360 m level in the Stripa mine and has previously been used for large scale permeability tests and thermal conductivity tests within the Swedish-American Cooperative Program on Radioactive Waste Storage in Mined Caverns in Crystalline Rock,(SAC), Lundström and Stille (1978).

Originally, there were two identical test sites in the drift, each consisting of 16 vertical boreholes evenly distributed on a circle with a radius of 1.5 metres. The holes were all 10 m deep with a diameter of 76 mm. In the centre of the circle, a vertical hole with a diameter of 300 mm was drilled. Two of the peripheral holes were core drilled all others percussion drilled.

Single hole tests performed within the SAC-project indicated that the inner test site, showing more anisotropic responses, would be most suitable for heterogeneity and migration studies. Location and geometry of the test sites is shown in figures 6 and 7. The preliminary hydraulic tests at the inner test site indicated considerably lower hydraulic conductivity in the centre hole than in the peripheral holes and the core drilled holes showed larger pressure responses than the percussion holes. This indicated that the percussion holes had been clogged by drilling debris and was not representative for the hydraulic conductivity at the site.

In view of this it was decided to modify the site. This was done by deepening 8 of the peripheral holes from 10 to 20 meters by diamond core drilling, Ø 76 mm, and deepening of the centre hole to 20 meters with diamond core drilling Ø 116 mm.

Several advantages were expected from the modification. The results would be representing undisturbed rock at 370-380 m

depth and should be uneffected by choosen drilling method.

The drill cores obtained valuable information about fractures, fracture systems and fracture fillings.

4.2 Geology

The target rock in the excavation is a grey to reddish, medium-grained granite of Precambrian age called Stripa granite. The petrology and lithology of the Stripa granite has been closely studied within the Stripa Project and the SAC-programme by Olkiewicz et al (1978, 1979), Koark and Lundström (1979), Wollenberg et al (1980) and Carlsson et al (1983).

The matrix of the granite consists of approximately 35-45 volume % of quartz, 35-40 % of partly sericitised plagioclase, 15-20 % of microcline and around 5 % of muscovite and biotite (altered to chlorite). Veins of pegmatite and aplite are common in the granite.

An elaborate fracture mapping of the drill cores has been made in order to identify fractures conducting water in an attempt to refind the fractures in neighbouring boreholes, see chapter 4.3 . The presence of fracture fillings has been studied for each fracture/fracture zone. Chlorite and calcite are the most dominating fracture filling minerals, occurring in about 80 % of all fractures, see table 3.1.a.

Table 3.1.a Fracture filling minerals

Mineral	Occurence (% of all fractures)
Chlorite	82
Calcite	78
Mica	33
Epidote	18
Pyrite	5
Fluorite	2
Others	24

4.3 Fracture correlation

From the core logs, a fracture frequency of 8 fractures/m was obtained. This relatively high fracture frequency made it difficult to correlate fractures and fracture zones between the holes. The 116 mm core from the centre hole was also to a large extent mechanically crushed during the drilling, which made it almost impossible to obtain any correlation with the centre hole.

However, most of the fractures are sealed by hydrothermal precipitations and very thin (< 1 mm) and are not involved in the transport of groundwater. It was therefore decided to concentrate on the 1-m sections with a hydraulic conductivity $K > 1$ E-10 m/s (see table 6.1.c) in the correlation attempts. Predictions of water conducting fractures and fracture zones was also made in these sections, mostly using fracture precipitations, e.g. rust, as indicators.

Table 4.3a shows the correlation attempts and prediction of water conducting fractures. The predicted water conducting fracture intervals are in good agreement with the results from the cross-hole tests and the tracer test, chapter 6.2 and 7.1 respectively.

Table 4.3.a Fracture correlation between boreholes and prediction of water conducting fracture intervals for sections with K > 1 E-10 m/s (- = no flow, ± = possible flow, + = probable flow).

Hole	Section depth (m)	Predicted intervals of conducting fractures	Correlated fractures
1	14-15	-	none
3	11-12	± 11.25 m	"
	17-18	+ 17.85-18.00 m	zone 17.85-18.00 m with hole 5 16.20-16.35 m
5	11-12	-	none
	12-13	-	"
	16-17	± 16.20-16.35 m	see hole 3, 17-18 m
	17-18	± 17.40-17.50 m	none
7	11-12	± 11.55 m	"
	12-13	-	"
	16-17	± 16.95-17.10	"
	17-18	± 16.95-17.10	"
9	12-13	-	"
	13-14	-	"
	16-17	+ 16.05-16.35	"
	17-18	+ 17.05-17.40	"
11	12-13	-	"
	14-15	± 14.70-14.80	"
	16-17	+ 16.45-16.55	"
13	12-13	-	"
	14-15	+ 14.90-15.00	"
	15-16	+ 15.30-15.50	"
	16-17	± 16.60-17.00	"
15	13-14	± 13.40	"
	15-16	-	"
	16-17	± 16.55-16.75	"

5. EQUIPMENT AND PROCEDURES

5.1 Single-hole tests

Equipment suitable both for the hydraulic testing and the tracer test has been designed, see figure 8. The injection of water is made by pressurizing the water in two pressure tanks, with nitrogen. The tanks are connected by three-way valves which makes it possible to refill the tanks without stopping the injection. The injection flow rate is measured with float type flow meters, ranging from 4 to 5200 ml/h, and the injection pressure by a manometer. The down-hole equipment consists of inflatable packers filled with water. The water is pressurized through a pressure tank by nitrogen. The centre hole packers and the peripheral hole packers has a length of 1.0 and 0.3 metres respectively.

The single-packer tests were performed in all nine holes by sealing off the boreholes at 11.0 metres depth with inflatable packers. The injection of water was made with a 20 m constant excess pressure for three hours. Flow rates and injection pressure were manually registered once a minute during the first 15 minutes and then with gradually increasing time intervals.

The double-packer tests were performed in 1.0 m sections from 10.0 metres to the bottom of the boreholes. The injections were made between two inflatable packers through a perforated steel tube. These tests were also made with a 20 m constant excess pressure, but for 20 minutes due to the large number of measurements to be performed. The registration procedure was the same as in the single-packer tests.

5.2 Cross-hole tests

The cross-hole tests were performed using the same equipment as in the single-hole tests (figure 8). The injection and monitoring intervals were equipped with pressure transducers situated immediately above the sealed-off sections and connected to them by nylon tubing. The transducer readings were recorded on two

stripchart recorders and also manually on voltmeters. A total of 9 double-packers with a pressure transducer each was assembled i.e. one for each peripheral hole and one for the injection hole. The centre hole was chosen for the injection hole as one of the purposes of this test was to compare it to the tracer test where the injection was made in the centre hole.

The injection section was selected by performing short injection tests in the three most responding sections in the centre hole. The section 16-17 metres having fast pressure responses in some of the peripheral holes, was chosen.The most high conductive sections in each peripheral hole were selected as monitoring sections. In order to fulfill the theoretical assumptions of treating the sections as points, it was decided to have 0.5 m-sections in the peripheral holes. This would also give better geometrical interpretations.

The main tests were conducted in the following sequence:

1)	Packer inflation	30 minutes
2)	Section pressure to equilibrium	12 hours
3)	Injection with constant excess pressure 30.0 m	6 hours
4)	Packer deflation and change of section	

A total of 23 sections were monitored using the same injection section in the centre hole. The configurations are shown in figure 9. Pressure changes below and above the monitoring sections were manually registered by checking the water level in nylon tubes connected to the lower sections and by checking the open water level in the boreholes respectively.

5.3 Tracer test

The equipment for the tracer test has been designed for 16 sampling sections, two in each peripheral hole with the packers at 11.0 and 15.8 metres depth.

The sampling equipment (figure 8) consists of a common time-step unit which operates 16 separate sampling units, each with 12 solenoid valves. The time-step unit controls the length of the time interval between sampling and also the opening time for the solenoid valves. The samples are taken directly in test tubes used at the analysis.

The water in the sampling sections is circulated during the test in order to keep homogeneous concentration at each time-step. The circulation is obtained by a small circulation pump connected to a buffer tank. The buffer tank is necessary because of the very low inflows to the sampling sections i.e. more water is taken out from the system than the inflow can compensate. The water level in the buffer tanks is used as a check of the volume in the sampling sections. The circulation capacity and tubing dimensions have been carefully selected to ensure that no excess pressure is created.

The injection equipment is identical with the equipment used for the hydraulic testing (fig 8). The flow is also checked by measuring the rate at which water level is lowered in the injection tanks. The section length used for the tracer injection was 9 metres (11.0-20.1 m depth).

The injection of tracer was preceded by about 7 weeks injection of water at 30.0 m excess pressure to obtain constant flow and pressure conditions. When steady state was obtained, a non-sorbing tracer, Uranine (sodium floureseine), was injected. The Uranine was dissolved in 0.2 m^3 water from borehole N1 at the 360 m level. The solution was contained in a 0.6 m^3 tank where complete mixing was established by a circulation pump. The tracer solution was pumped out at the bottom of the water filled centre hole and the original, non-labelled water was pressed up in the tank and mixed with the tracer solution. This

procedure continued for about one hour until a homogeneous solution was obtained. The circulation then was stopped and injection started with 31 m excess pressure.

Samples were taken, at 2 hour intervals in the beginning and then at gradually increasing intervals up to 16 hours, from all 16 sampling sections. All the samples were analysed by spectrophotometry. In order to increase the detectability and accuracy at low concentrations, the early breakthrough samples were measured by fluorometry. This method increased the detectability about 100 times.

6. RESULTS OF HYDRAULIC TESTS

6.1 Results of single-hole tests

The hydraulic conductivity, K(m/s), has been determined in all 9 holes by single packer tests in the interval 11.0 - 20.0 m and by double-packer tests with 1.0 m section length from 10.0 to 20.0 m depth. The hydraulic conductivity of the centre hole and the sampling sections used at the tracer test were tested both before and after the tracer test in order to study possible changes with time.

The three hour single packer tests were evaluated using the transient analysis in equation (4). The results are presented in table 6.1.a and figure 10.

Table 6.1.a Hydraulic conductivity from single-packer tests, peripheral holes

Hole no	Section (m)	K (m/s)
1	11.0-19.9	5.6E-11
3	11.0-20.0	8.3E-11
5	11.0-20.0	1.4E-10
7	11.0-20.0	2.8E-10
9	11.0-20.0	1.2E-10
11	11.0-20.0	5.5E-11
13	11.0-20.0	4.6E-10
15	11.0-20.0	4.5E-11

The conductivity of the centre hole has been determined at 3 different times. First, immediately after the drilling (830121), secondly before the tracer test (830420) and third after the tracer test (840120). The results in table 6.1.b show a clear decrease of hydraulic conductivity probably due to clogging effects.

Table 6.1.b Hydraulic conductivity from single-packer tests, centre hole section 11.0-20.0 m.

Date	K (m/s)
830121	1.7E-10
830420	8.0E-11
840120	9.0E-12

The measure limit of the single-packer equipment was 5 E-12 m/s.

The double-packer tests in 1.0 m-sections were also evaluated as transient tests by eq (4). The centre hole was sealed off with a packer at 11.0 m depth and pressure responses below the packer due to the injection in the peripheral holes could be monitored by checking the water level in a standpipe. The results from the double-packer measurements are shown in table 6.1.c and figures 11.a and 11.b. Sections marked with R were responding in the centre hole during the injection.

In order to make comparisons between single- and double-packer tests the transmissivity, T (m^2/s), was calculated for the interval 11.0-20.0 m in all 9 holes, respectively using:

$$T = \Sigma K_i \cdot L_i \qquad (42)$$

where K_i = hydraulic conductivity in section i (m/s)
L_i = length of section i (m)

Table 6.1.d shows the calculated values, the mean and standard deviation of the transmissivity calculated from eq (42).

Table 6.1.c Double-packer tests

Hole no	Section (m)	K (xE-11 m/s)		Hole no	Section (m)	K (xE-11 m/s)	
1	10-11	1.8		11	10-11	1.4	
	11-12	3.7			11-12	1.2	
	12-13	1.3			12-13	13.9	
	13-14	3.8			13-14	1.8	
	14-15	32.5			14-15	14.8	
	15-16	3.9			15-16	3.9	
	16-17	2.0			16-17	13.6	
	17-18	0.9			17-18	1.8	
	18-19	1.1			18-19	1.5	
	18.45-19.45	1.2			18.6-19.6	1.6	
3	10-11	38.9		13	10-11	38.7	
	11-12	24.8			11-12	1.1	
	12-13	1.7			12-13	26.0	
	13-14	13.4			13-14	2.2	
	14-15	3.7			14-15	81.0	R
	15-16	2.9			15-16	69.3	
	16-17	1.3			16-17	36.3	
	17-18	29.1	R		17-18	1.9	
	18-19	1.3			18-19	1.6	
	18.6-19.6	1.4			18.67-19.67	0.7	
5	10-11	1.8		15	10-11	114.0	
	11-12	10.7			11-12	1.3	
	12-13	30.5			12-13	1.0	
	13-14	0.9			13-14	20.7	
	14-15	1.0			14-15	9.8	
	15-16	3.4			15-16	12.1	
	16-17	39.4			16-17	24.4	
	17-18	23.1			17-18	4.3	
	18-19	1.7			18-19	1.0	
	18.57-19.57	1.6			18.67-19.67	1.0	
				CENTRE			
7	10-11	2.1			11-12	27.6	
	11-12	12.8			12-13	3.4	
	12-13	30.4			13-14	5.7	
	13-14	1.2			14-15	21.3	
	14-15	1.1			15-16	49.0	
	15-16	20.4			16-17	22.8	
	16-17	53.1			17-18	13.8	
	17-18	11.6			18-20.1	0.8	
	18-19	2.6					
	18.6-19.6	1.8					
9	10-11	67.3					
	11-12	1.4					
	12-13	16.8					
	13-14	18.7					
	14-15	1.4					
	15-16	1.4					
	16-17	40.5	R				
	17-18	20.0					
	18-19	2.1					
	18.6-19.6	2.0					

Table 6.1.d Transmissivity from single-hole tests with single- and double-packer equipments

Hole no	Section (m)	T single (x E-10 m^2/s)	T double (x E-10 m^2/s)	T double/T single
1	11.0-19.9	5.0	5.0	1.00
3	11.0-20.0	7.5	8.0	1.07
5	11.0-20.0	12.5	11.2	0.90
7	11.0-20.0	24.8	13.5	0.54
9	11.0-20.0	10.7	10.4	0.97
11	11.0-20.0	5.0	5.4	1.08
13	11.0-20.0	41.6	22.0	0.53
15	11.0-20.0	4.0	7.6	1.90
CENTRE	11.0-20.1	15.3	14.5	0.95
Mean value		14.0	10.8	0.77
Standard dev.		12.2	5.3	0.40

The ratio T double/T single is very close to 1.0 in 7 out of 9 holes, indicating good agreement between the two different tests. However the two most high conductive holes, 7 and 13, differ more. This is probably due to the short registration time in the double-packer tests which tends to underestimate the hydraulic conductivity in the high conductive sections.

After the tracer test was completed, the hydraulic conductivity of the sampling sections was determined again to trace clogging effects in the sections as experienced from the hydraulic conductivity determinations in the centre hole. The tests were made in the same way as the previous double-packer tests using a constant head injection, but for 30 minutes this time. The transient analysis was made using equation (4) and the hydraulic conductivity values were transfered into transmissivity using equation (42). The results shown in table 6.1.e, indicates a decrease in transmissivity in 7 of the 8 monitoring holes. As T before, the value from the three hour single-packer test was used.

Table 6.1.e Transmissivity before and after tracer injection

Hole no	T before (x E-10 m^2/s)	T after (x E-10 m^2/s)	T after/T before
1	5.0	1.6	0.32
3	7.5	5.4	0.72
5	12.5	6.9	0.55
7	24.8	8.1	0.33
9	10.7	6.7	0.63
11	5.0	3.0	0.60
13	41.6	56.4	1.36
15	4.0	3.8	0.95
Mean	13.9	11.5	0.83
Std. dev.	13.1	18.3	0.34

6.2 Results from cross-hole tests

The cross-hole tests were conducted between the section 16.00-17.00 metres in the centre hole and 23 different sections within the 8 peripheral holes. The locations of the sections are shown in figure 9. The sections were selected from the results of the single-hole tests in 1-m sections, the core logs and the results of the tracer test.

The length of the injection and monitoring sections, 1.0 and 0.5 m respectively, were chosen to meet the assumptions that the sections could be treated as points. The validity of this assumption could be checked by the equations (17) and (18). Rough estimates of α_1 and β_1 can be made by assuming $K_d(\underline{e}_1) = K_d(\underline{e}_b) = K_d(\underline{e})$ i.e. small degree of anisotropy. Then (17) and (18) reduces to R/L > 2.5 and R/B > 2.5, respectively. As the distances between injection and monitoring sections are in the order of 1.5-3.5 meters, the criterion is fulfilled for the monitoring sections but in some cases not for the injection section. However, the flow from the injection section is probably occuring from a single major fracture or a small fracture zone within the 1-m section.

Thus, it seems reasonable to represent this interval as a point source. This is also indicated by the good fit to the type-curves.

Table 6.2.a shows the results from the type-curve matching for all sections monitored. Pressure responses were registered in 11 of the 23 monitoring sections with a range of 0.03-0.63 metres after six hours of injection. All the responses were registered within 5 minutes after start of injection.

Table 6.2.a Results from cross-hole tests, injection interval 16.00-17.00 m in centre hole

Hole no	Monitoring Interval (m)	Matched Values * $(\Delta h)R_j/Q$ (s/m)	t/R_j^2 (s/m^2)	Computed Values ** $K_d(\underline{e}_j)/D$ (s^2/m^2)	$K_d(\underline{e}_j)/S_s$ (m^2/s)	D/S_s (m^4/s^3)
1	14.20-14.70	***	***			
	16.50-17.00	***	***			
3	17.00-17.50	***	***			
	17.50-18.00	1.38 E9	340	3.01 E20	2.94 E-3	9.79 E-24
	18.00-18.50	***	***			
5	16.50-17.00	***	***			
	17.00-17.50	7.20 E7	3600	8.19 E17	2.78 E-4	3.39 E-22
	17.50-18.00	***	***			
7	16.30-16.80	4.30 E8	950	2.92 E19	1.05 E-3	3.61 E-23
	16.80-17.30	5.00 E8	3750	3.95 E19	2.67 E-4	6.76 E-24
	17.30-17.80	6.30 E8	960	6.27 E19	1.04 E-3	1.66 E-23
9	16.50-17.00	5.50 E8	1350	4.78 E19	7.41 E-4	1.55 E-23
	17.00-17.50	6.00 E8	1120	5.69 E19	8.93 E-4	1.57 E-23
	17.50-18.00	8.00 E8	5000	1.01 E20	1.01 E-4	1.98 E-24
11	14.30-14.80	***	***			
	15.50-16.00	***	***			
	16.20-16.70	7.80 E8	4750	9.61 E19	2.11 E-4	2.19 E-24
13	15.50-16.00	***	***			
	16.00-16.50	***	***			
	16.50-17.00	***	***			
15	13.00-13.50	***	***			
	16.00-16.50	7.20 E8	2450	8.19 E19	4.08 E-4	4.99 E-24
	16.50-17.00	6.40 E8	1830	6.47 E19	5.46 E-4	8.45 E-24

* values matched to $h_{PD} = 1$ and $t_{PD} = 1$
** computed by equations (12) and (13)
*** no response within 6 hours

The validity of treating the rock as a homogeneous anisotropic porous medium could be checked as described in chapter 2.2 by examing, 1) the fit of the type curves, 2) the range of D/S_s and 3) the polar plot of $(K_d(\underline{e}_j)/S_s)^{1/2}$ versus $\underline{e}_j$.

The fit of the type-curves is shown in figures 12 a-d. The fits are in general not good for the early time data due to the injection at constant pressure instead of constant flow rate, but after about one hour of injection the fit becomes good in all cases except for hole no 5. The response in hole no 5 is in the order of cm:s and could also be resulting from non-stabilized background pressure. This value has therefore not been included in the calculations. The values of D/S_s from table 6.2.a are all within a factor of 20 except for hole no 5, which also indicates that the assumption is valid.

The plots of $(Kd(\underline{e}_j)/S_s)^{1/2}$ versus the directions $\underline{e}_j$ in figures 13.a and 13.b are constructed in two planes as a three-dimensional plot is difficult to construct. The plot in figure 13.a is constructed in a horizontal plane. As most of the responding sections are located within a horizontal plane ($\pm 20^o$), all the values of $(K_d(\underline{e}_j)/S_s)^{1/2}$ versus $\underline{e}_j$ have been plotted in figure 13.a. A reasonably good fit can be made to the five points located in the horizontal plane. However, in holes no 1, 5 and 13 there is no response within this plane which makes the interpretation questionable. In figure 13.b a vertical plane between holes no 7 and 15 have been constructed, but no good fit can be made.

An attempt has also been made to fit the data to an ellipsoid by an ordinary least square procedure. However this has not been successful as the solution have failed to become positive definite. This is probably due to the fact that the responding sections are located almost in a plane and that the scatter of the data is too large.

The conclusion of these tests is that the rock cannot be treated as a homogeneous anisotropic porous medium in this scale. However, the tests can be used to quantify directional hydrau-

lic diffusivities within discrete fractures and to indicate the locations of possible transport paths.

The results presented in figure 14 shows that fractures have large variations in directional hydraulic diffusivities over short distances. This is in agreement with preliminary results from crosshole sinusoidal measurements in Stripa, Black (1985).

7. RESULTS OF TRACER TEST

7.1 Flow and residence time

The results from the tracer test can be divided into three categories:

1) Results from the first 500 hours of injection with increasing flow rates in all sampling sections carrying tracer

2) Results from 500-1876 hours of injection with decreasing flow rates in some of the sections

3) Results from 1876-2535 hours of injection with no continuous sampling and no circulation of the water in the sampling sections

The reason for this division is that the flow rate distribution was totally changed when the continuous sampling and circulation was stopped after 1876 hours of injection as could be seen in Table 7.1.a. During the continuous sampling, all sampling sections had the same constant hydraulic head created by the circulation procedure but when the circulation was stopped, the natural hydraulic head distribution was obtained in the sampling sections, thus creating a new flow rate distribution. This, together with results from the hydraulic tests indicates that the transport takes place in different channels within a few well-connected fracture planes. Which channels depends on the hydraulic head distribution in the fracture planes.

The decreasing flow rates after about 500 hours of injection is probably due to either leakage around the packer in the injection hole or increasing flow rate in one or several channels not penetrating the sampling sections.

The injection flow rate was almost constant, 26-28 ml/h, during the entire experiment and the maximum total flow rate to the sampling sections was 2.4 ml/h which makes about 8 % recovery of injected tracer. Sampling was also made in the 10 m deep

peripheral holes not used at the test and in the open sections above the sampling sections.

Table 7.1.a Flow rate distribution at three different times in the peripheral holes

Borehole section	Q (500 h) (ml/h)	Q (1876 h) (ml/h)	Q (2535 h) (ml/h)
1 L	-	-	-
1 U	-	-	-
3 L	0.39	0.22	0.03
3 U	-	-	-
5 L	-	-	0.68
5 U	-	-	0.05
7 L	-	-	-
7 U	-	-	-
9 L	0.62	0.42	0.18
9 U	-	-	-
11 L	0.14	0.10	-
11 U	-	-	0.01
13 L	0.33	0.33	-
13 U	0.33	0.07	0.85
15 L	0.59	0.48	-
15 U	-	-	0.04
TOTAL	2.40	1.62	1.84

L = Lower section
U = Upper section
- = no flow

Tracer was detected in holes no 9 and 12 with flow rates of 0.50 and 0.05 ml/h respectively, making up about 2 % of the injected flow rate. Thus, the total recovery was 10 %.

All of the following calculations have been made using the results from the increasing part of the flow rate curves, i.e. from the first 500 hours of injection.

The flow rates calculated from the slopes of the breakthrough curves as described in chapter 3.1, were very low, 0.14-0.62 ml/h, distributed into 2-3 channels within the sampling sections (table 7.1.b). The corresponding residence times were between 38 and 420 hours. All the breakthrough curves are shown in figures 15 a-c. Figure 16 shows an enlargement of the breakthrough to section 15 L showing the interpretation of the residence time t_0 and the flow rate q to the section.

Table 7.1.b Flow rates and residence times of Uranine

Section	q (ml/h)	Q (ml/h)	t_o (h)	t_o (h)
3 L	0.16		50	
	0.23	0.39	90	74
9 L	0.22		38	
	0.17		85	
	0.23	0.62	250	130
11 L	0.09		180	
	0.05	0.14	380	251
13 L	0.12		150	
	0.13		230	
	0.08	0.33	420	250
13 U	0.23		75	
	0.10	0.33	160	101
15 L	0.23		95	
	0.16		170	
	0.20	0.59	310	188

q = channel flow rate, Q = total flow rate

7.2 Hydraulic fracture conductivity

The hydraulic fracture conductivity, K_e, has been calculated with both radial and linear flow assumptions and with the flow rate, q, and residence time, t_o, as basic variables. The results are presented in table 7.1.c for radial and linear flow respectively.

Table 7.1.c Hydraulic fracture conductivity with radial and linear flow assumptions.

Section	K_e^t (x E-7 m/s)		K_e^q (x E-7 m/s)		K_e^q / K_e^t	
	rad	lin	rad	lin	rad	lin
3 L	6.5	3.7	110	49	17	13
	3.6	2.1	140	62	38	30
9 L	8.6	4.9	136	60	16	12
	3.9	2.2	114	51	30	23
	1.3	0.7	140	62	107	83
11 L	1.8	1.0	75	33	41	32
	0.9	0.5	51	22	59	46
13 L	2.2	1.2	91	40	42	32
	1.4	0.8	96	42	67	52
	0.8	0.4	69	31	89	69
13 U	4.4	2.5	140	62	32	25
	2.0	1.2	80	36	39	31
15 L	3.4	2.0	140	62	41	32
	1.9	1.1	110	49	57	45
	1.1	0.6	127	57	121	94
Mean value	2.9	1.7	108	48	53	41
Stand. dev	2.2	1.3	30	13	31	24

A comparison between radial and linear flow indicates that the radial flow assumption gives about 2 times higher values than the linear assumption. However, the difference between K_e^t

and K_e^q, here expressed as the ratio K_e^q/K_e^t, is very similar, a factor 40-50.

The K_e^q/K_e^t ratio has been found to increase with increasing residence time. The data indicate a linear increase with the logarithm of residence time (figure 17):

Radial flow: $K_e^q/K_e^t = 80 \cdot \log t_o - 120$

Linear flow: $K_e^q/K_e^t = 63 \cdot \log t_o - 94$

The correlation is 0.81 for both equations. The difference between K_e^q and K_e^t is not surprising as they represent two different ways of describing the hydraulic property of fractures as discussed in chapter 3.2. K_e^t represents the volume of the flow path where the particles are delayed in the "lakes" of the fracture, resulting in longer residence times. The delay can also be resulting from diffusion into the rock matrix and at this stage it is not possible to conclude which process is dominating. The K_e^q-values are determined only from the flow rates to the sampling sections thus representing the most narrow paths of the fracture.

7.3 Flow porosity

The flow porosity, θ_k, has been calculated in the two different ways described in chapter 3.3.

The hydraulic conductivity ratio, θ_{kk}, in equation (36) was calculated using the hydraulic fracture conductivity K_e^t from equation (30) and the rock mass hydraulic conductivity K, was determined as the mean value of the conductivities in the sampling sections and the centre hole.

The volumetric based flow porosity, θ_{kv}, in equation (37) was calculated with t_o as a weighted mean value:

$$\bar{t}_o = \frac{q_1}{q_{tot}} \cdot t_{01} + ... + \frac{q_n}{q_{tot}} \cdot t_{on} \qquad (43)$$

where $q_1, \ldots q_n$ = channel flow rates
q_{tot} = total flow rate
$t_{o1}, \ldots t_{on}$ = channel residence times

The results are:

$\theta_{kk} = 3.8$ E-4
$\theta_{kv} = 6.7$ E-5

These values are one order of magnitude lower than reported by Gustafsson and Klockars (1981) in a high conductive fracture zone ($k_e = 3$ E-3 m/s) in Finnsjön. Gale and Rouleau (1983) calculated flow porosities from laboratory data on apertures in Stripa granite from the same area as this investigation. Their results indicated flow porosities in the order of 1 E-5.

7.4 Dispersion

The scale factor is of great importance when the dispersion parameter is determined. In a small scale, the dispersion within individual flow paths can be studied and in larger scales the dispersion within fracture networks. In the scale of this investigation it was difficult to calculate the dispersivity within individual flow paths due to insufficient resolution in the breakthrough data. However, it can be concluded from the breakthrough curves that the dimensionless dispersion parameter $n < 0.01$ for individual flow paths i.e. very low dispersivity within the distance of 1.5 metres. Instead, the mean residence time, t_o, and n was determined by fitting equation (40) to the experimental data for the total flow to the sampling sections. This dispersion is caused by the different hydraulic properties in the different flow paths and is termed macrodispersion.

In a larger scale, like the tracer tests in Finnsjön, Gustafsson and Klockars (1981), where the distance is 30 meters between injection and sampling section and the hydraulic conductivity is much higher, the macro dispersion could be interpreted

as dispersion within individual flow paths. Thus, it is of great importance to specify in which scale the dispersion parameter has been determined when comparisons are made.

The results of the calculations are shown in table 7.4.a. The fit to the theoretical curves was made by transforming the breakthrough curves to relative concentration C/C_o versus time from equation (23). However, this calculation could not be made for sections 3 L and 9 L due to the scatter in the early breakthrough data. The results from sections 11 L, 13 L, 13 U and 15 L shown in table 7.4.a and figure 18 indicate good agreement with the t_o determinations by weighted mean values presented in table 7.1.b.

Table 7.4.a Mean residence time, t_o, and dimensionless dispersion parameter, n

Section	t_o (h)	n	no of flow paths
3 L	*	*	2
9 L	*	*	3
11 L	240	0.03	2
13 L	300	0.08	3
13 U	90	0.05	2
15 L	130	0.08	3

* no fit possible

The n values are very low and increasing with increasing number of flow paths as expected. The scale dependency could be identified by comparing the results from Finnsjön, where n = 0.03 - 0.05 for individual flow paths, to the values in table 7.4.a for several flow paths. The macro dispersion parameter in Finnsjön was calculated to n = 0.3 i.e. 10 times higher than in Stripa.

7.5 Channeling

The channeling effect has been clearly shown by the tracer test, where a change in hydraulic head distribution gave rise to a completely different flow distribution. The tracer test and the cross hole tests indicate that the flow occurs within a few well connected fracture planes. However, at this stage it can not be concluded whether the channeling occurs within a single fracture or if it is a result of flow through several fractures.

Assuming that each flow channel, interpreted from the break-through curves, is an individual fracture, an estimate of the percentage water conducting fractures can be made. In table 7.5.a, the total number of water conducting fractures intersecting each hole is presented. The sections which responded after the completion of the continuous sampling (1876 h) are also included. Occurrence of tracer in these sections has been assumed to represent one water conducting fracture.

Table 7.5.a Number of water conducting fractures in the peripheral holes

Hole no	No. of water conducting fractures
1	0
3	2
5	2
7	0
9	3
11	3
13	5
15	4

Thus, a total number of 19 water conducting fractures was found, distributed within the 8 peripheral holes making up 0.26 water conducting fractures/m, i.e. a spacing of approximately 3.9 metres between the conducting fractures.

From the fracture mapping, a fracture frequency of 8 fractures/m was found. This means that the water conducting fractures are on an average 3 % of the total number of fractures.

With the assumption that the maximum number of 5 fractures (hole no 13) are involved in the transport of water from the injection hole, the active area, regarding the flow, can be estimated as described in chapter 3.5.

From table 7.5.a we conclude that 4 of the 8 peripheral holes have three or more water conducting fractures i.e. $Pr(x>3) = 0.5$. Thus, the probability of observing three or more flow channels is 50 %. Assuming that the number of observed water carrying fractures are binomially distributed and substituting the observation probability p, from equation (41), results in p 0.5, i.e. the active area of a fracture plane is about 50 % of the total area.

The maximum number of water conducting fractures, n, of equation (41) is an uncertain parameter in our data. Increasing n to 8 and 12 respectively, instead of 5, then $Pr(x>3)$ is found to be 0.3 and 0.2, respectively. It is seen that the probability and hence the active area of the fracture plane is still within the same order of magnitude.

The statistical representativity of the pheripheral holes as sampling points could be checked by comparing the recovery of tracer to the sampling area. The 8 peripheral holes with a diameter of 76 mm, together make up 6.5 % of the total mantle area of the cylindrical test arrangement and the total recovery in the sampling sections was 8 %. In combination this suggests that the peripheral holes together are statistically representative samples of the mantle area. However, it should also be pointed out that the statistical material is small.

8. DISCUSSION AND CONCLUSIONS

8.1 Experimental design

The cylindrical geometry of the test site with the injection hole in the centre offers several advantages:

- The heterogeneity of the rock can be studied by cross-hole tests in several directions.

- A valuable statistical material on fracture frequencies, fracture fillings and percentage water conducting fractures can be obtained.

- Tracer breakthrough can be monitored in several directions at the same distance from the injection point, giving information of heterogeneities, fracture geometry, statistical material on hydraulic fracture conductivity, flow porosity and dispersivity.

Injection of tracer with constant excess pressure is easier to perform than injection with constant flow. If steady state conditions prevail when tracer is introduced, the flow will be constant. Thus it is important to maintain steady state conditions by injecting water prior to the tracer injection.

There are also some difficulties with the performance of tracer tests in low conductive rock. The thin fractures with very low flow rates (0.01-1.0 ml/h) are sensitive to clogging especially at long injection times. Thus, it is important to use water from the same aquifer and to keep it pressurized under reducing conditions to prevent chemical clogging. The hydraulic head in the sampling sections should be kept constant as the flow geometry is governed by small variations in the head distribution along a fracture plane.

8.2 Hydraulic tests

The small scale of the test site made it possible to perform a detailed hydraulic test programme.
The single hole tests with constant excess pressure give valuable information about possible water conducting sections and is the first natural step when tracer tests are designed. The short injection period (20 minutes) makes the constant head tests especially attractive when a large number of tests are made.

The crosshole test is a useful tool to determine flow paths between boreholes and to quantify directional hydraulic diffusivities. However in the conductivity range and the scale of this experiment, it is not possible to assume a homogeneous, porous, anisotropic medium.

The results from the hydraulic tests can be summarized as follows:

- The hydraulic conductivity, K, from single hole tests (1 m-sections) varies between 1 E-9 - 7 E-12 m/s.

- A comparison between three hour single packer tests and 20 minutes double-packer tests shows very good agreement for the low conductive sections. However, the short time double-packer tests seem to under-estimate the hydraulic conductivity for highly conductive sections resulting in differences of a factor 2 in the transmissivity calculations.

- Clogging effects, resulting in decreasing hydraulic conductivity has been clearly shown by single-hole tests before and after the tracer test. The decrease is a factor of 20 in the injection hole and a factor of 1.1 - 3 in 7 of the 8 monitoring holes. Hole no 13 has an increased hydraulic conductivity which is probably due to an uncertain evaluation of the most conductive zone (8.1 E-10 m/s).

- The type curve fit to the cross-hole test was very good, however no hydraulic conductivity tensor could be determined due to lack of responses in different directions. This indicates that the rock cannot be treated as a homogeneous, anisotropic, porous medium in this scale and conductivity range.

- Directional hydraulic diffusivities, K_d/S_s, has been calculated. All directions are near horizontal ($\pm 20^o$) and K_d/S_s ranges between 2.9 E-3 - 1.0 E-4 m^2/s.

- The cross-hole tests have proved to be of valuable help in indicating possible flow paths or channels.

8.3 Tracer test

Tracer breakthrough was monitored in a total of 10 sections. Six of the sections were continuously sampled and could be evaluated with respect to hydraulic fracture conductivity, K_e, flow porosity, θ, and dispersion parameter, n. From the other four sections only the flow rate could be calculated.

The flow distribution in the cylinder was very heterogeneous and changed markedly during the injection when the continuous sampling and mixing was stopped. This indicates good hydraulic connection between the sampling sections and that the flow rate distribution is affected by small variations in the hydraulic head. In summary, the results indicate that the transport of water takes place within a few fractures. These fracture planes probably intersect all sampling holes but they are more or less open resulting in very different flow rates and residence times in each borehole. In some cases there was no flow at all, i.e. channeling occured.

The results from the tracer test can be summarized as follows:

- A total tracer recovery of 10 % was monitored within 10 sampling sections.

- The flow rates were very low, 0.14-0.62 ml/h, distributed into 2-3 channels within the sampling sections.

- The residence times for different channels varies between 38-420 hours.

- The hydraulic fracture conductivity, K_e, was calculated in two different ways, with the residence time, t_o, and the flow rate, q, as basic variable respectively, for both radial and linear flow. The mean values for linear flow are: K_e^t = 1.7 E-7 m/s and K_e^q = 4.8 E-6 m/s. The radial flow assumption gives about 2 times higher values for both calculation ways.

- The ratio, K_e^q/K_e^t was found to be time dependent. This probably results from the fact that K_e^t represents the volume of the fracture while K_e^q represents the most narrow paths of the fracture. The diffusion may also give similar effects on the calculations.

- The flow porosity, θ_k, was calculated in two different ways, as a volumetric ratio, θ_{kv}, and as a conductivity ratio, θ_{kk}. The results are θ_{kk} = 3.8 E-4 and θ_{kv} = 6.7 E-5.

- The dimensionless longitudinal dispersion parameter, n = 0.03 - 0.08 for the total flow to the sampling sections. For individual fractures $n < 0.01$.

- The water conducting fractures are on an average 3 % of the total number of fractures.

- Channeling has been observed.

- The "active area", defined as the area of a fracture where transport takes place, has been estimated to 50 % of the total area from calculations of probability.

REFERENCES

Abelin, H., Neretnieks, I., Tunbrant, S and Moreno, L., 1985: Final Report of the Migration in a Single Fracture-Experimental results and evaluation. Stripa Project Technical Report 85-03, Stockholm.

Black, J.H., 1985: Crosshole Investigations - Preliminary Results of Single-Borehole Hydraulic Test and Early Crosshole Sinusoidal Measurements. Paper at the NEA Information Symposium on in situ experiments in granite associated with the disposal of radioactive waste, Stockholm and Stripa June 4-6, 1985.

Carlsson, L., Olsson, T., Andrews, J., Fontes, J-C., Michelot, J.L. and Nordström, K., 1983: Geochemical and isotope characterization of the Stripa groundwaters - Progress report. Stripa project 83-01.

Gale, J.E. and Rouleau, A., 1983: Characterizing and interpreting the geometry, permeability and porosity of fractures for repository evaluation. Symp. on Field Measurements in Geomechanics, Zürich .

Gustafsson, E. and Klockars, C-E., 1981: Studies on groundwater transport in fractured crystalline rock under controlled conditions using non-radioactive tracers. SKBF/KBS Technical Report TR 81-07. Stockholm.

Gustafsson, E. and Klockars, C-E., 1984: Study of strontium and cesium migration in fractured crystalline rock. SKBF/KBS Technical Report TR 84-07. Stockholm.

Hsieh, P.A., Neuman, S.P. and Simpson, E.S., 1983: Pressure Testing of Fractured Rocks - A Methodology Employing Three-Dimensional Cross-Hole Tests. U.S. Nuclear Regulatory Commission Report NUREG/CR-3213.

Hsieh, P.A., and Neuman, S.P., 1985: Field Determination of the Three-Dimensional Hydraulic Conductivity Tensor of Anisotropic Media, 1. Theory. Submitted to Water Resources Research.

Hsieh, P.A., Neuman, S.P., Stiles, G. K. and Simpson, E.S., 1985: Field Determination of the Three-Dimensional Hydraulic Conductivity Tensor of Anisotropic Media, 2. Methodology and Application to fractured Rocks. Submitted to Water Resources Research.

Koark, H.J. and Lundström, I., 1979: Berggrundskartan Lindesberg SV. SGU Ser Af 126. Stockholm.

Landström, O., Klockars, C-E., Holmberg, K. and Westerberg, S., 1978: In situ experiments on nuclide migration in fractured crystalline rocks. KBS Technical Report TR 100. Stockholm.

Landström, O., Klockars, C-E., Persson, O., Torstenfelt, B., Allard, B., Tullborg, E-L. and Larson, S.Å., 1983: Migration experiments in Studsvik. SKBF/KBS Technical Report TR 83-18. Stockholm.

Lundström, L. and Stille, H., 1978: Large scale permeability test of the granite in the Stripa mine and thermal conductivity test, Swedish-American Cooperative Program on Radioactive Waste Storage in Mined Caverns in Crystalline Rock. Techn. Proj. Report no 2, LBL-7052.

Norton, D. and Knapp, R., 1977: Transport phenomena in hydrothermal systems: the nature of porosity. Am. Journal of Science, Vol 277, Oct. 1977, p 913-936.

Ogata, A. and Banks, R., 1961: A Solution of the Differential Equation of Longitudinal Dispersion in Porous Media, U S Geol. Surv. Prof. Paper 411-A, Washington.

Olkiewicz, A., Hansson, K., Almén, K-E. and Gidlund, G., 1978: Geologisk och hydrologisk dokumentation av Stripa försöksstation KBS Technical Report TR 63. Stockholm.

Olkiewicz, A., Gale, J.E., Thorpe, R. and Paulsson, B., 1979: The geology and fracture system at Stripa. LBL-8907. SAC -21.

Snow, D.T., 1968: Rock fracture spacings, openings, and porosities. J. Soil Mech. Found. Div. Proc. ASCE, Vol. 94, No SM 1.

Uraiet, A.A. and Raghavan, R., 1980: Pressure buildup analysis for a well produced at constant bottomhole pressure. J. Pet. Tech. (Oct. 1980), pp 1813-1824.

Walton, W.C., 1970: Groundwater Resource Evaluation. McGrawHill Book Company, New York.

Wollenberg, H., Flexser, S. and Andersson, L., 1980: Petrology and radiogeology of the Stripa pluton. LBL-11654.

Zuber, A., 1974: Theoretical possibilities of the two-well pulse method, Isotope Techniques in Groundwater Hydrology 1974 (Proc. Symp. Vienna, 1974), IAEA, Vienna.

APPENDIX A NOMENCLATURE

A	(m^2)	area
C		concentration
C_o		initial concentration
$C(t)$		concentration at time t
D_l	(m^2/s)	longitudinal dispersion coefficient
D	(m^3/s^3)	determinant of hydraulic conductivity tensor $\underline{K}$
e	(m)	mean fracture width
$\underline{e}$		unit vector
$\underline{e}_j$		unit vector in the direction of j-th observation point
$\underline{e}_l$		unit vector parallel to injection interval
$\underline{e}_b$		unit vector parallel to monitoring interval
g	(m/s^2)	acceleration due to gravity
H_o	(m)	excess pressure
h	(m)	hydraulic head
$\underline{h}$	(m/m)	hydraulic gradient
h_{PD}		dim. less hydraulic head defined by eq (12)
h_j	(m)	hydraulic head at j-th observation point
K	(m/s)	hydraulic conductivity
$\underline{K}$	(m/s)	hydraulic conductivity tensor
$K_d(\underline{n})$	(m/s)	directional hydraulic conductivity
$K_d(\underline{e}_j)$	(m/s)	directional hydraulic conductivity
K_e	(m/s)	hydraulic fracture conductivity
$\underline{n}_T$		unit vector
$\underline{n}$		transpose unit vector
$n = D/vx$		dimensionless dispersion parameter
$Q(t)$	(m^3/s)	flow at time t
Q_c	(m^3/s)	injection flow rate
$\underline{q}$	(m^3/s)	specific discharge
q	(m^3/s)	channel flow rate
R_j	(m)	distance between point source and j-th observation point
R	(m)	distance between injection and monitoring interval
r	(m)	radius
r_w	(m)	well radius

S		storage coefficient
S_s	(m^{-1})	specific storage
T	(m^2/s)	transmissivity
t	(s)	time
t_D		dimensionless time defined in eq (5)
t_{pD}		dimensionless time defined by eq (13)
t_o		mean residence time of water
$\underline{U}$		matrix defined by eq (15)
v	(m/s)	velocity
V	(m^3)	volume
V_w	(m^3)	volume of water
V_r	(m^3)	volume of rock
x		cartesian coordinate
z		stochastic variable
α_1		dimensionless parameter defined by eq (18)
β_1		dimensionless parameter defined by eq (20)
ν	(m^2/s)	kinematic viscosity
θ_T		total porosity
θ_k		kinematic porosity
θ_{kk}		kinematic porosity defined by eq (36)
θ_{kV}		kinematic porosity defined by eq (37)
θ_d		diffusion porosity
θ_r		residual porosity
∇_o		divergence operator
∇		gradient operator

LIST OF ILLUSTRATIONS

Fig 15 a-c Breakthrough curves for Uranine in sections 3 L, 9 L, 11 L, 13 L, 13 U and 15 L.

Fig 16 Breakthrough curve section 15 L showing the interpretation of q and t_o.

Fig 17 $K_e{}^q/K_e{}^t$ versus log t_o.

Fig 18 a-b Expertimental breakthrough curve for Uranine and fit with theoretical curves for sections 11 L, 13 L 13 U and 15 L.

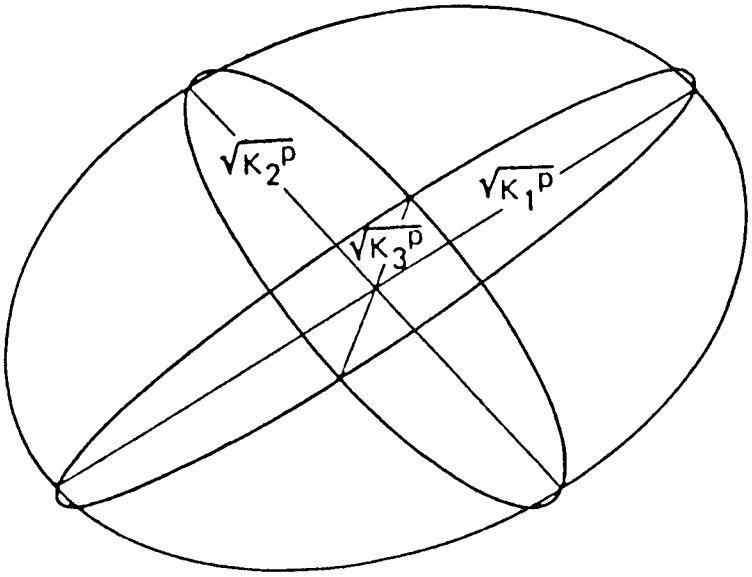

Fig 1 Directional hydraulic conductivity ellipsoid (From Hsieh et al 1985).

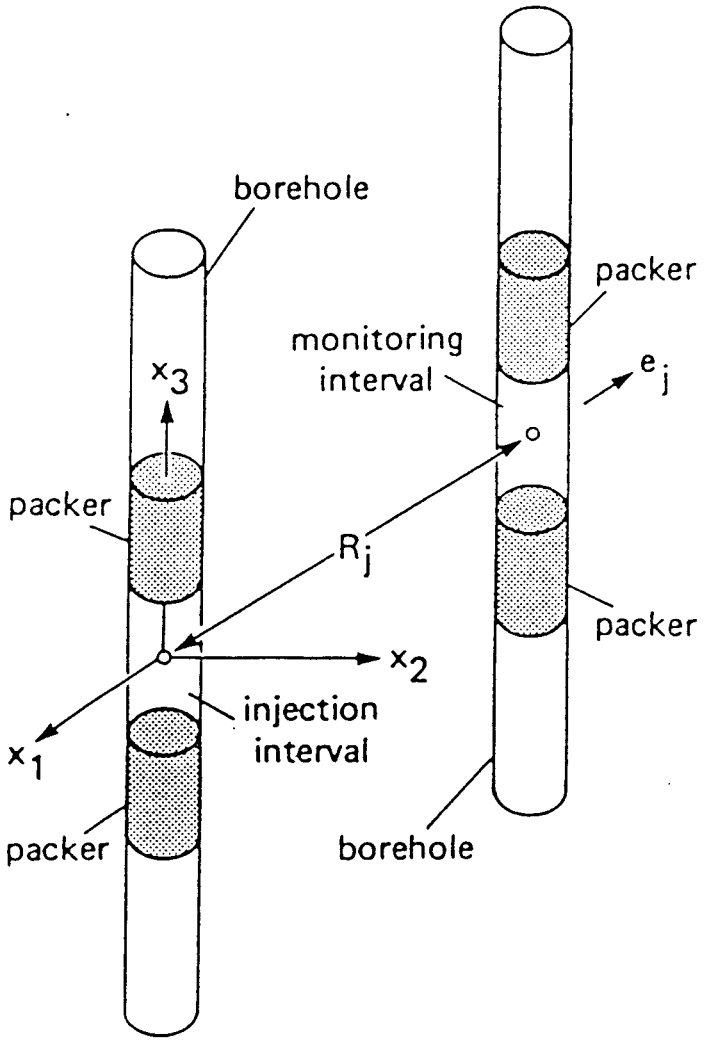

Fig 2 Spatial relationship between the injection and observation intervals (From Hsieh et al 1985).

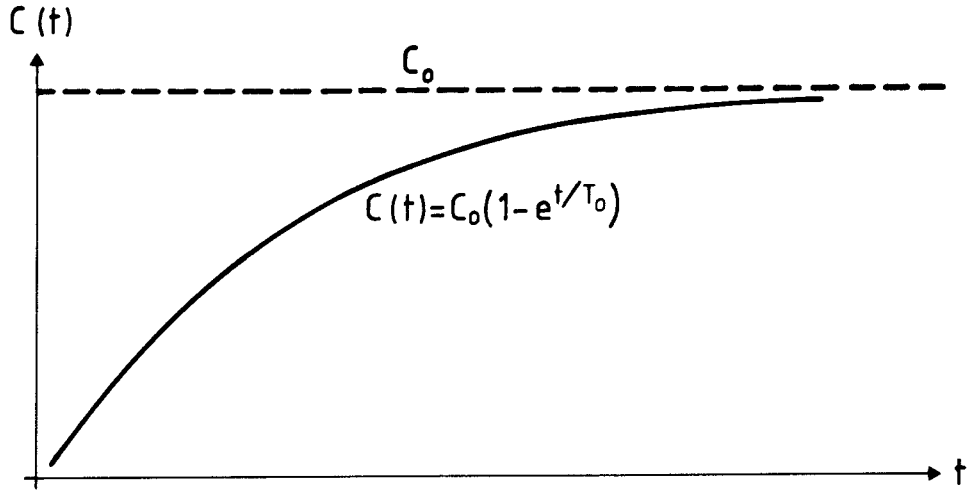

Fig 3 Solution to the continuity equation (21) assuming complete mixing.

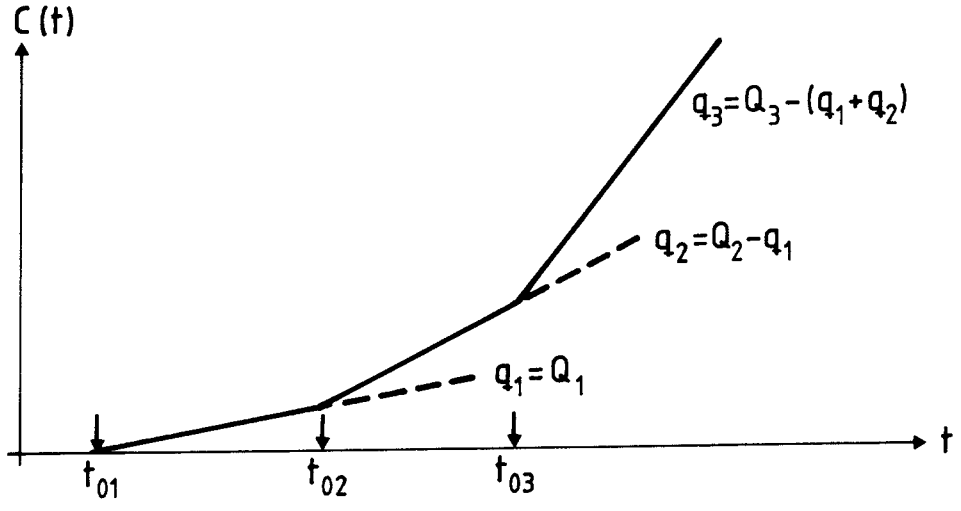

Fig 4 Breakthrough curve with three flow channels.

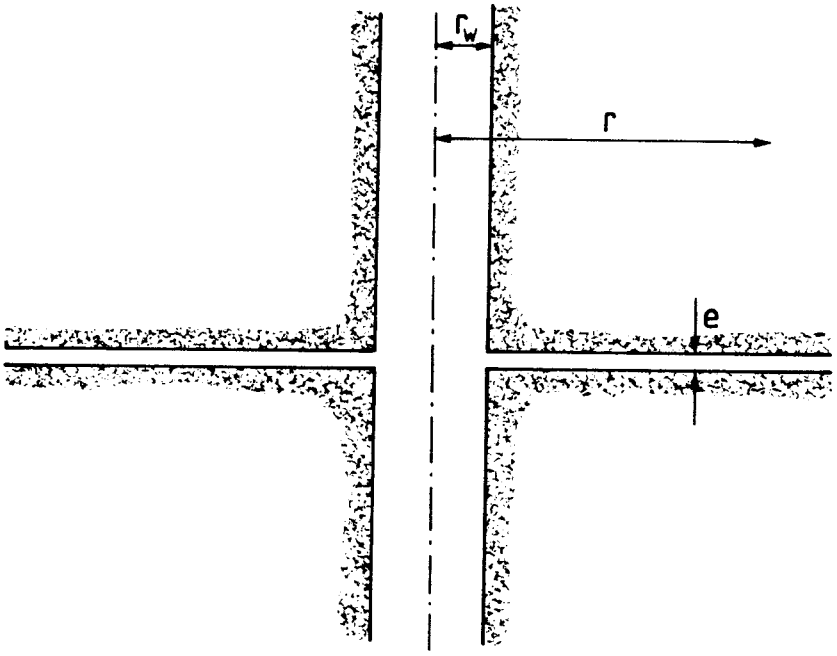

Fig 5 Radial flow from a borehole with radius r_w through a fracture with fracture width e.

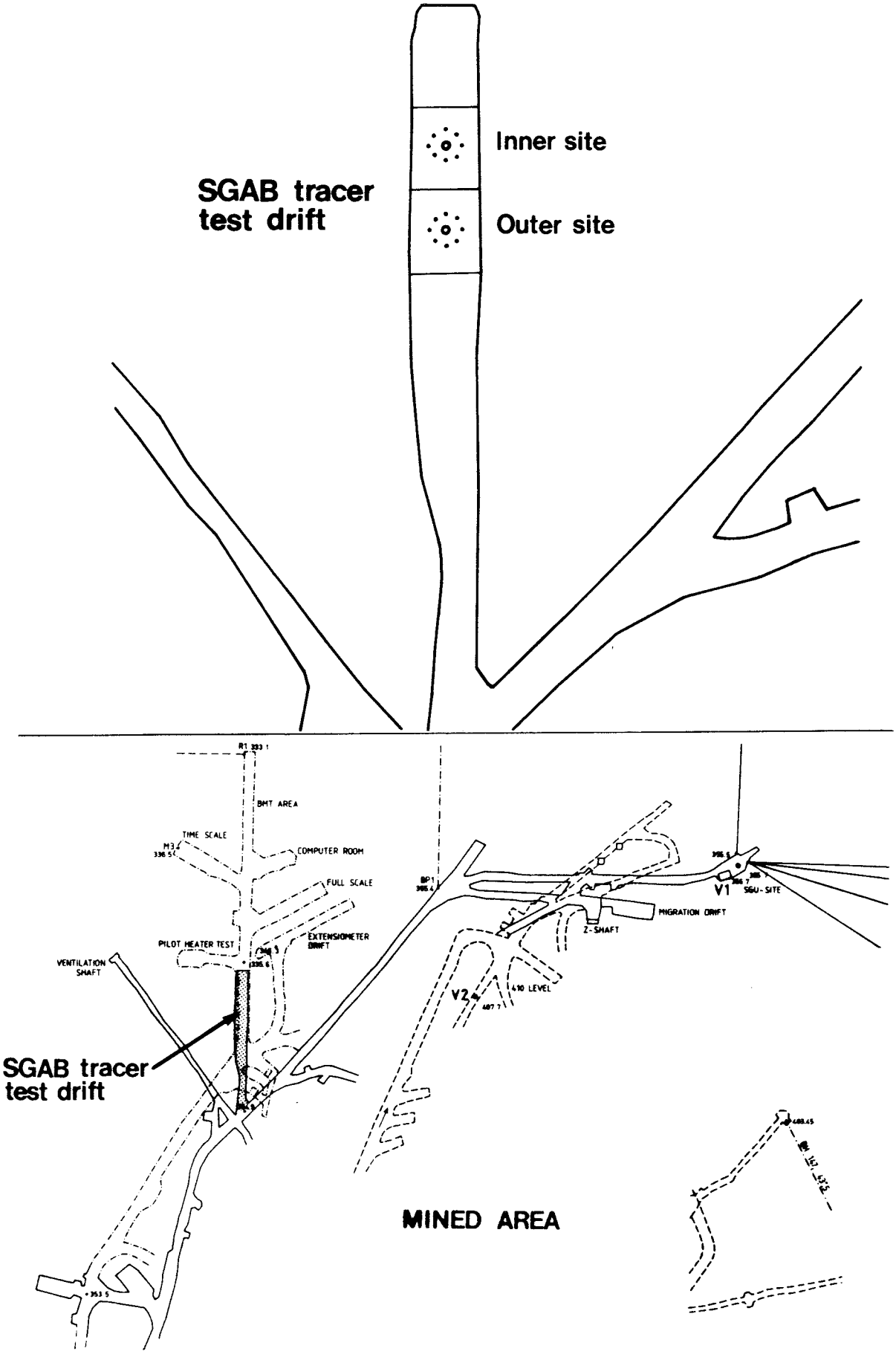

Fig 6 Test site location at 360 m level in the Stripa mine.

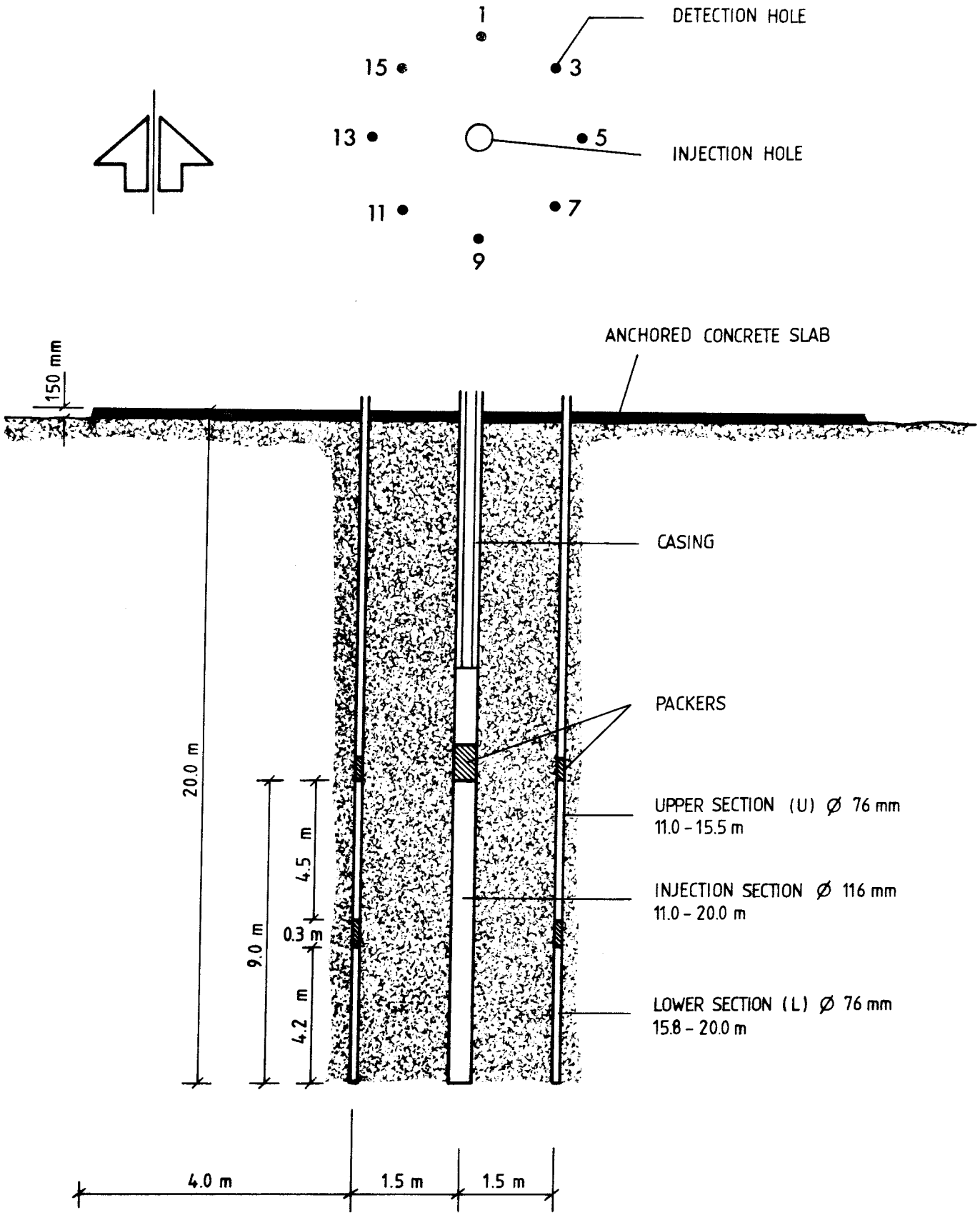

Fig 7 Geometry of the test site.

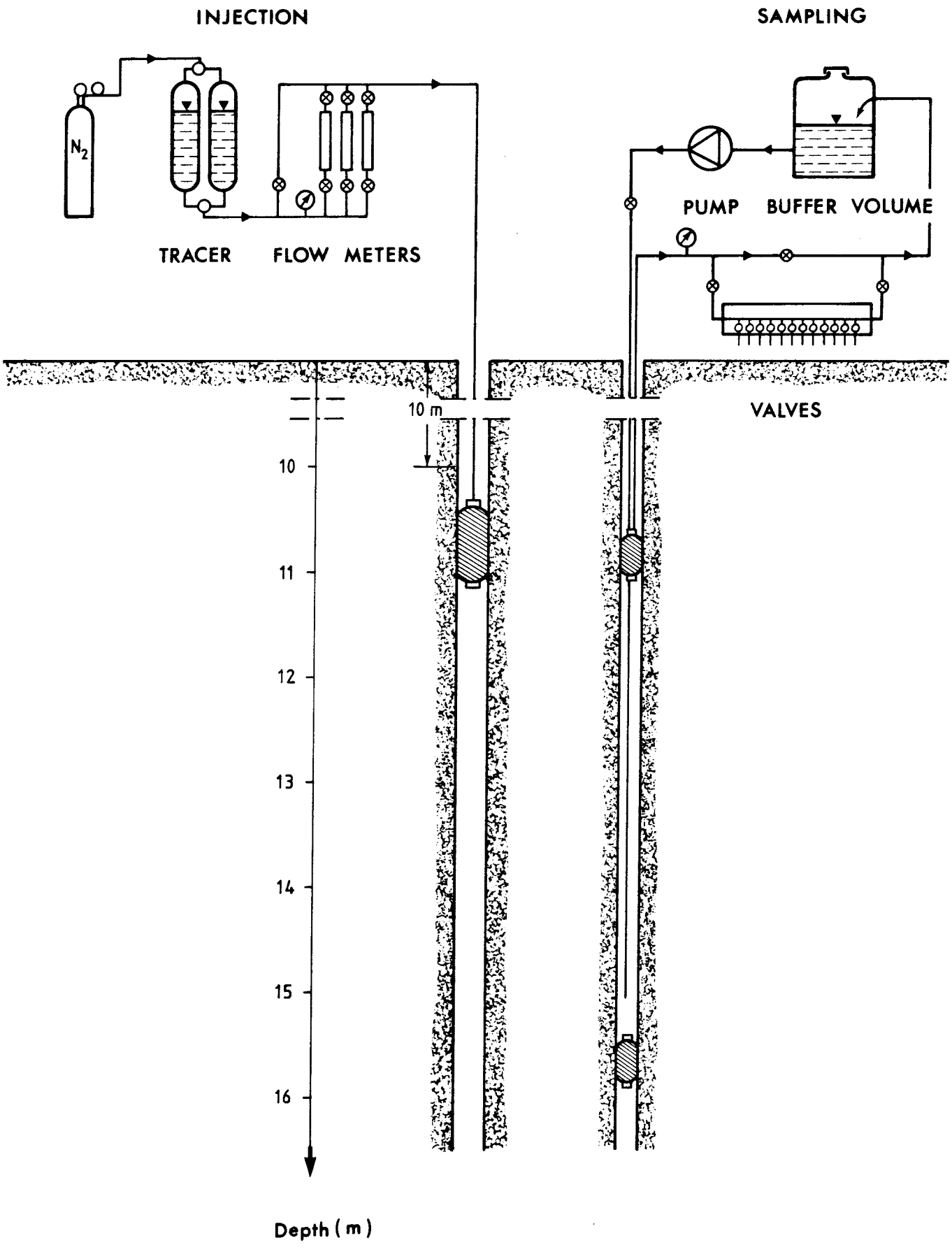

Fig 8 Injection and sampling equipments.

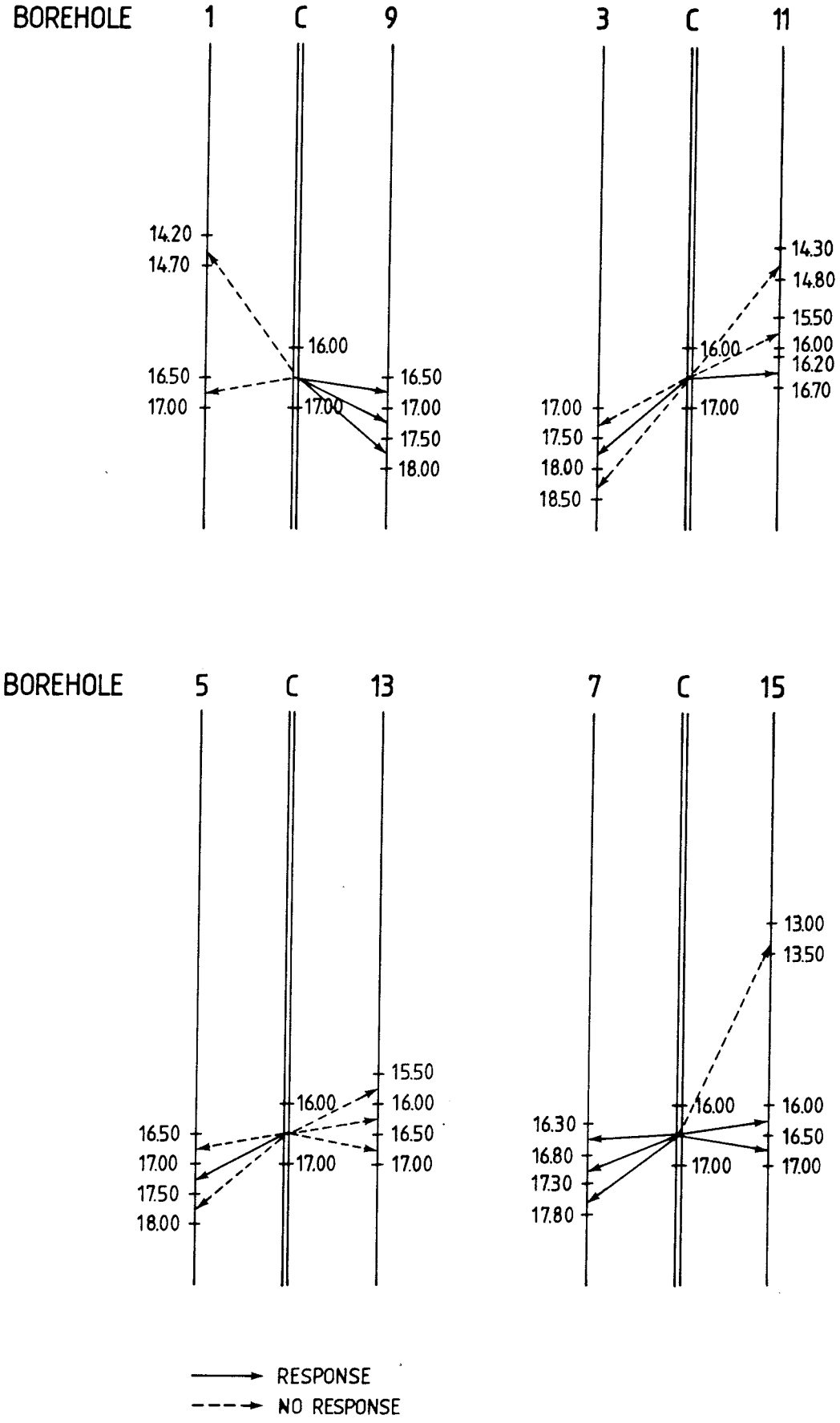

Fig 9 Injection and monitoring intervals chosen for the cross-hole tests.

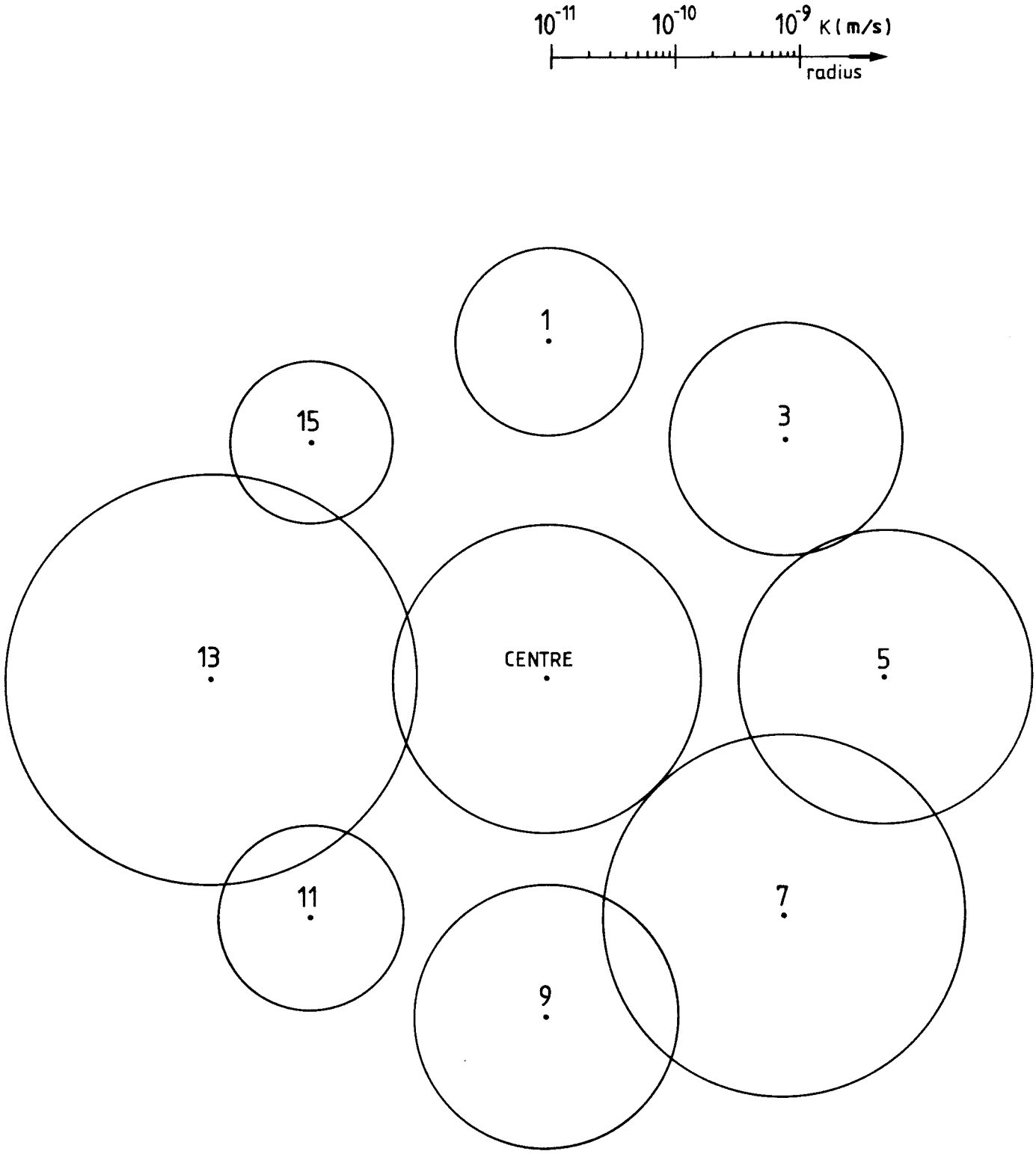

Fig 10 Hydraulic conductivity from single-packer tests, section 11.0-20.0 m.

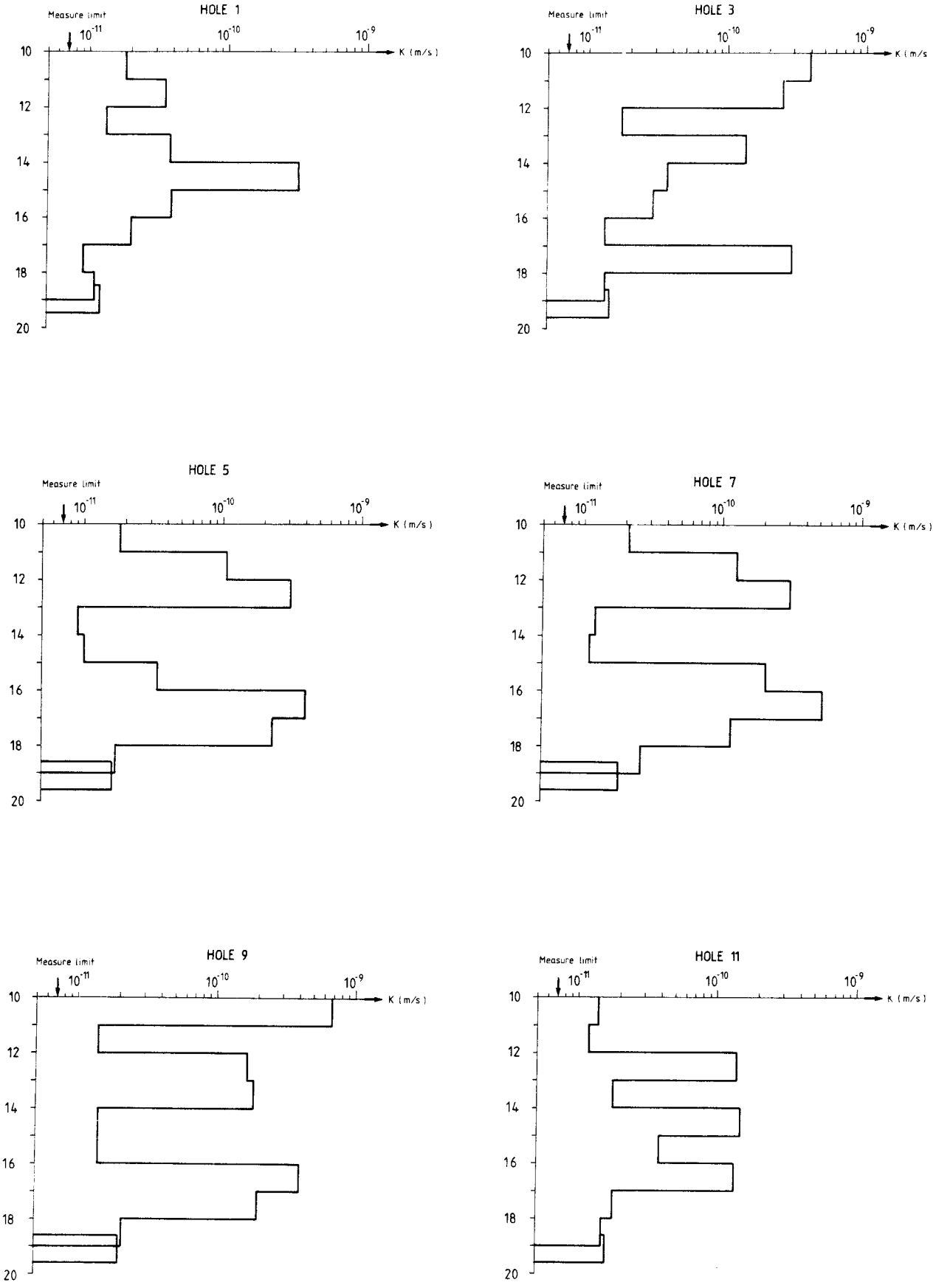

Fig 11a Hydraulic conductivity from double-packer tests, 1.0 m sections, for holes no 1, 3, 5, 7, 9 and 11.

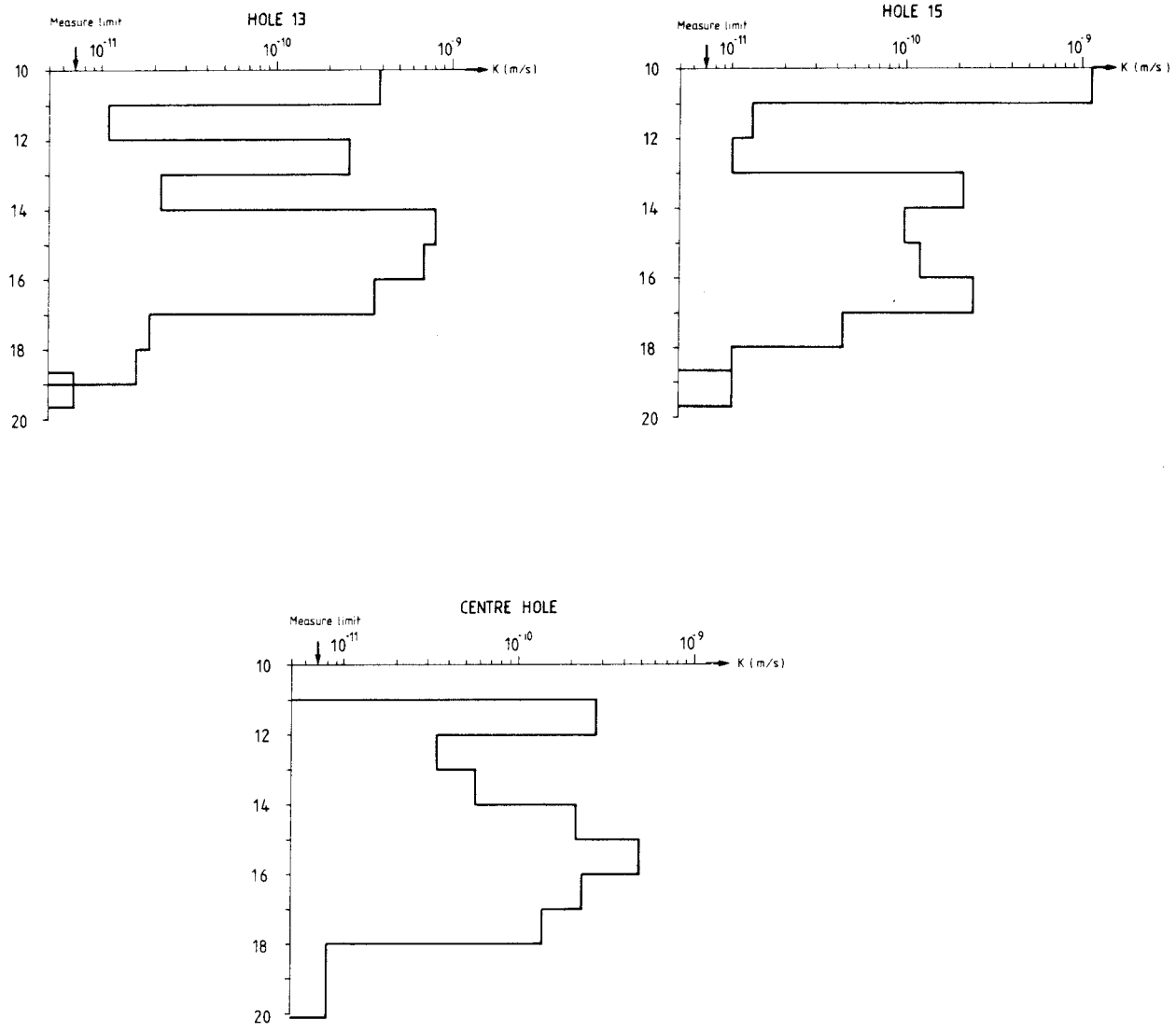

Fig 11b Hydraulic conductivity from double-packer tests, 1.0 m sections, for holes no 13, 15 and centre hole.

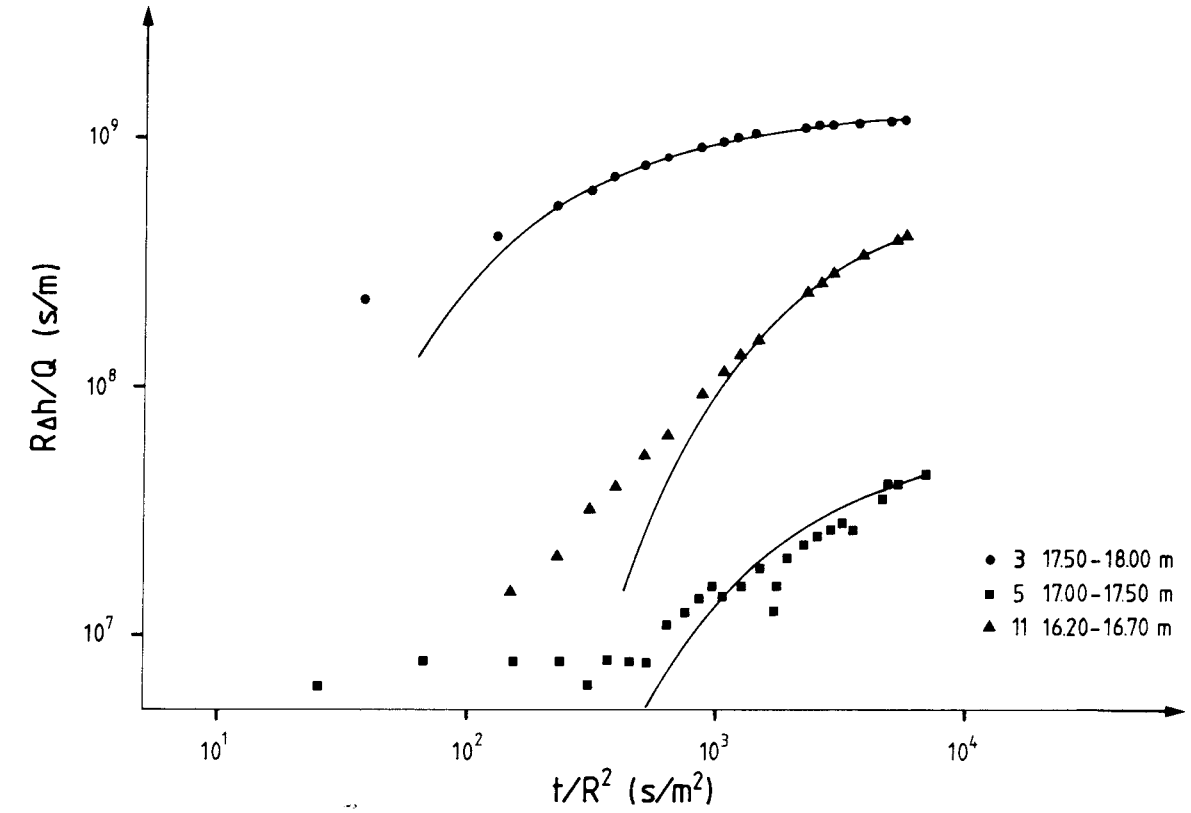

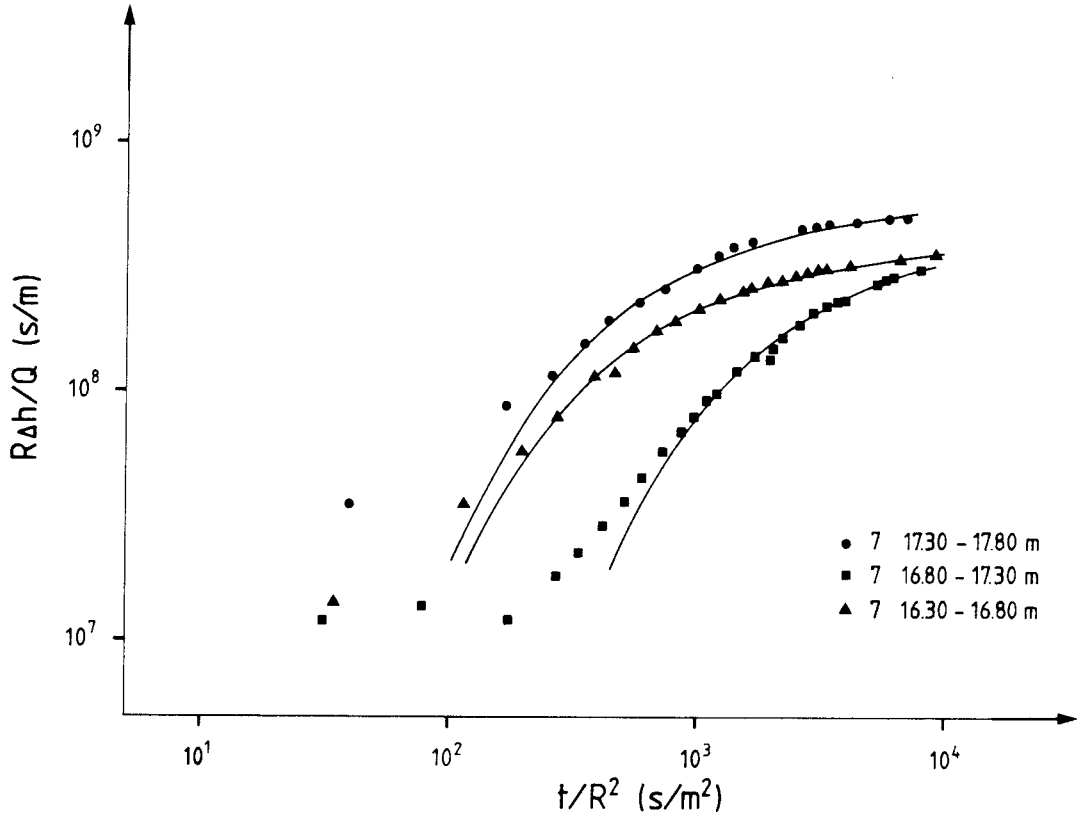

Fig 12a Data plots of $R\Delta h/Q$ versus t/R^2 and fitted type curves from cross-hole tests.

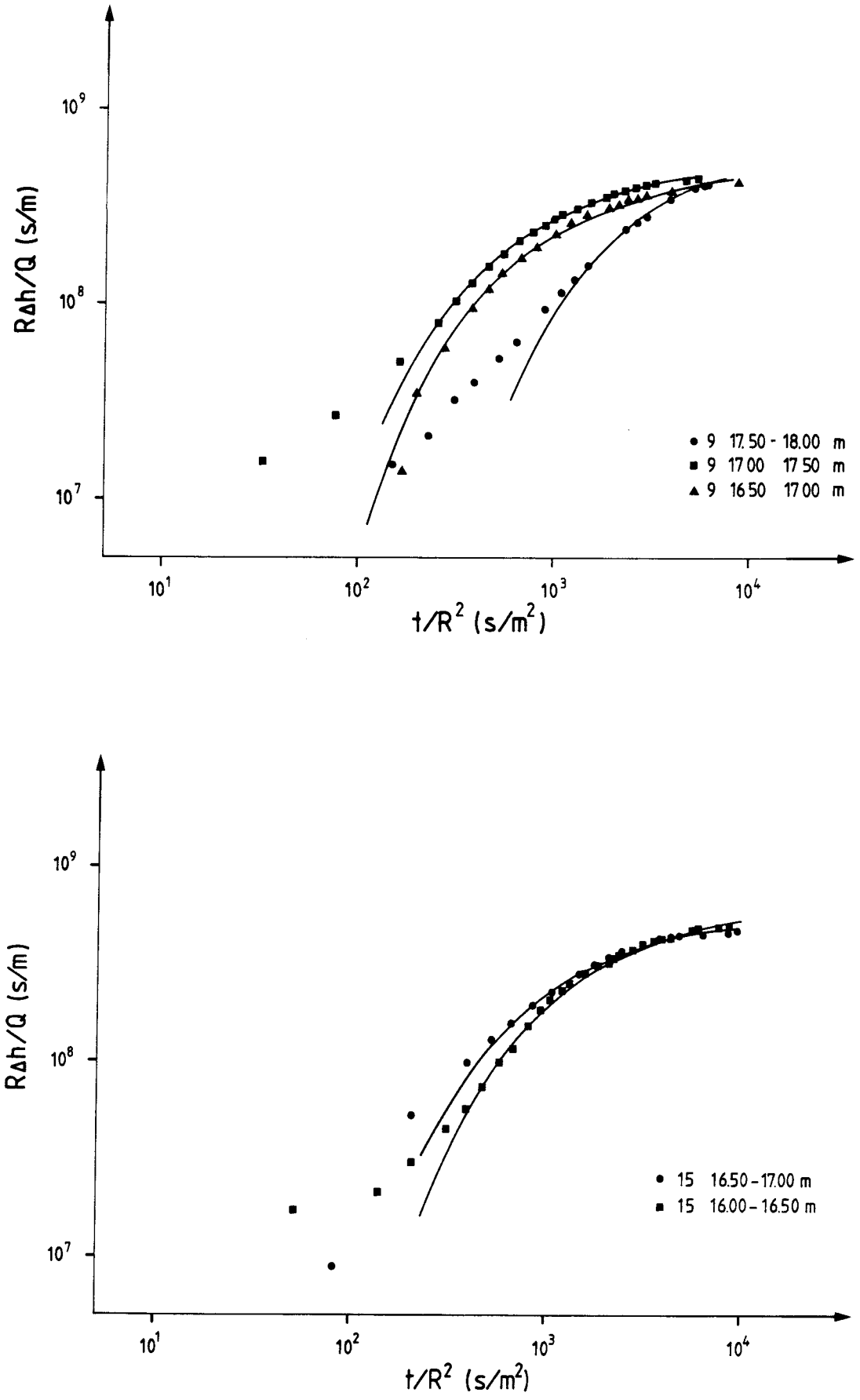

Fig 12b Data plots of RΔh/Q versus t/R^2 and fitted type curves from cross-hole tests.

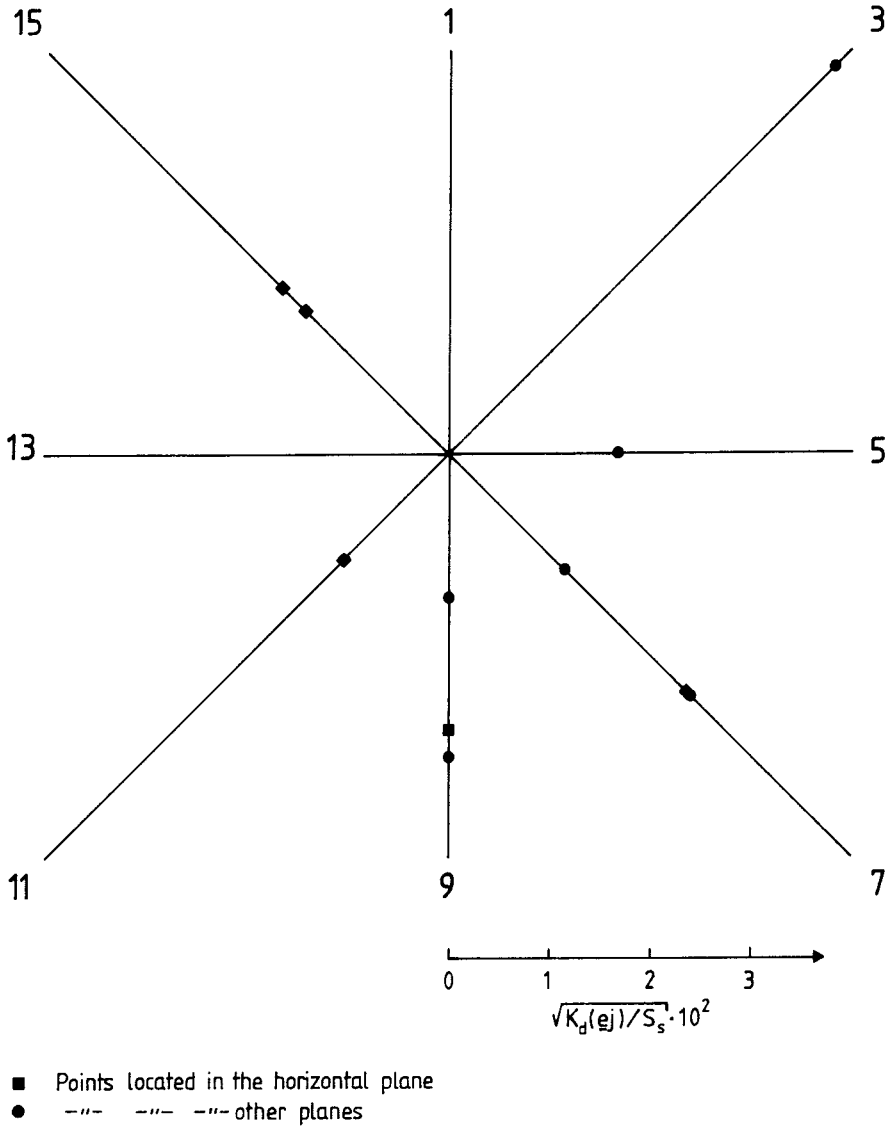

Fig 13a Polar plot of $(K_d(\underline{e}_j)/S_s)^{1/2}$ versus the directions $\underline{e}_j$ in a horizontal plane.

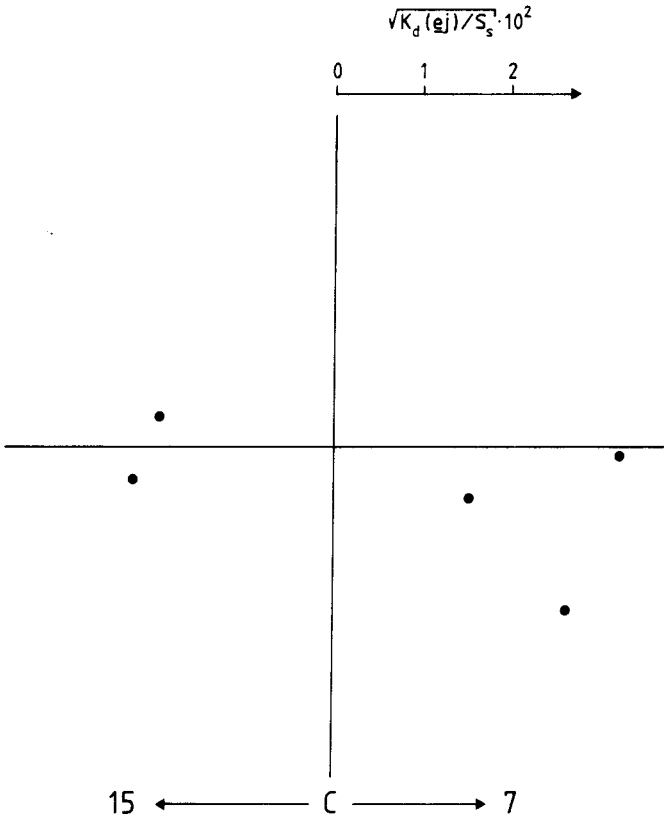

Fig 13b Polar plot of $(K_d(\underline{e}_j)/S_s)^{1/2}$ versus the directions $\underline{e}_j$ in a vertical plane between boreholes 7 and 15.

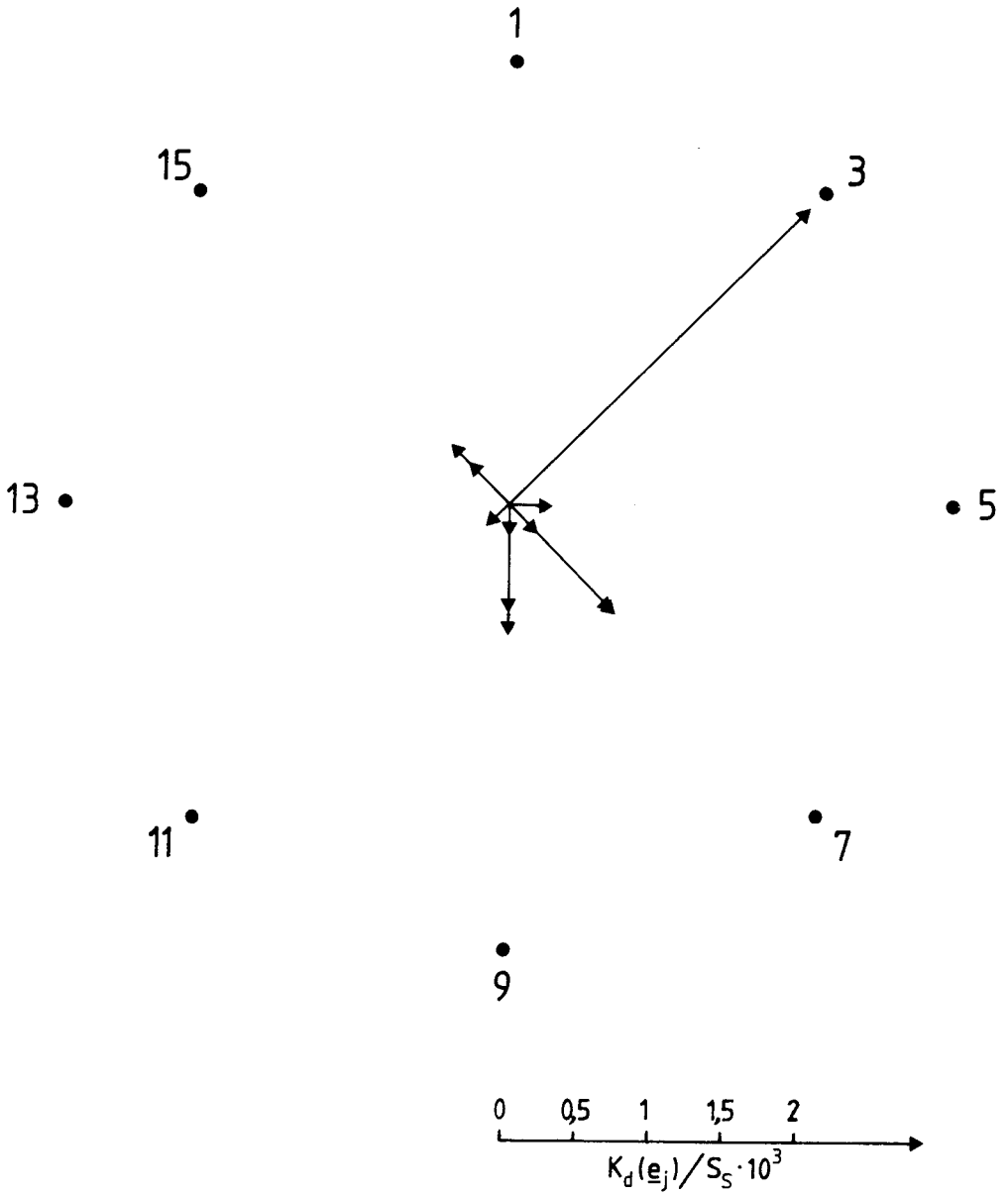

Fig 14 Directional hydraulic diffusivities plotted in a horizontal plane.

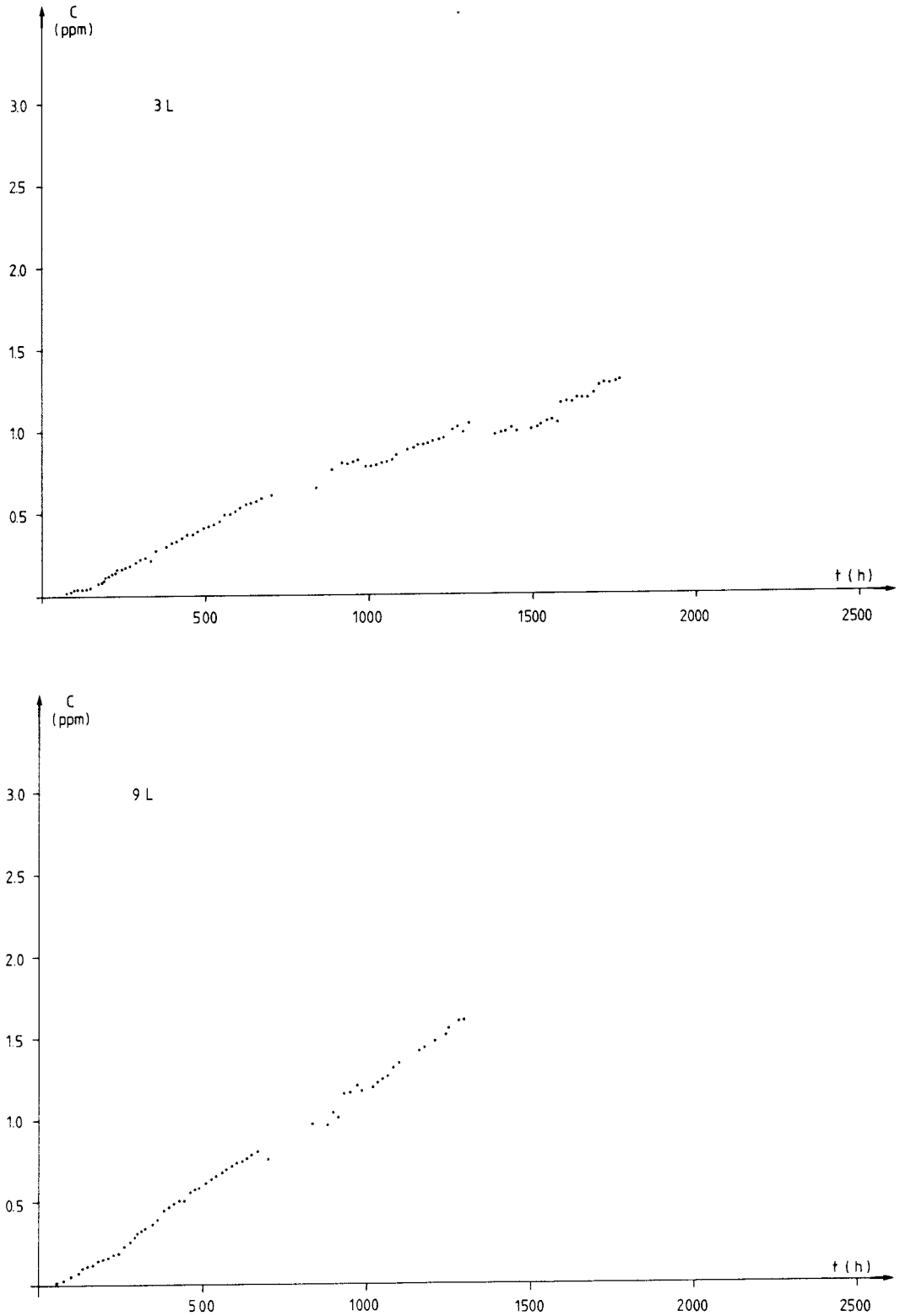

Fig 15a Breakthrough curves for Uranine in sections 3 L and 9 L.

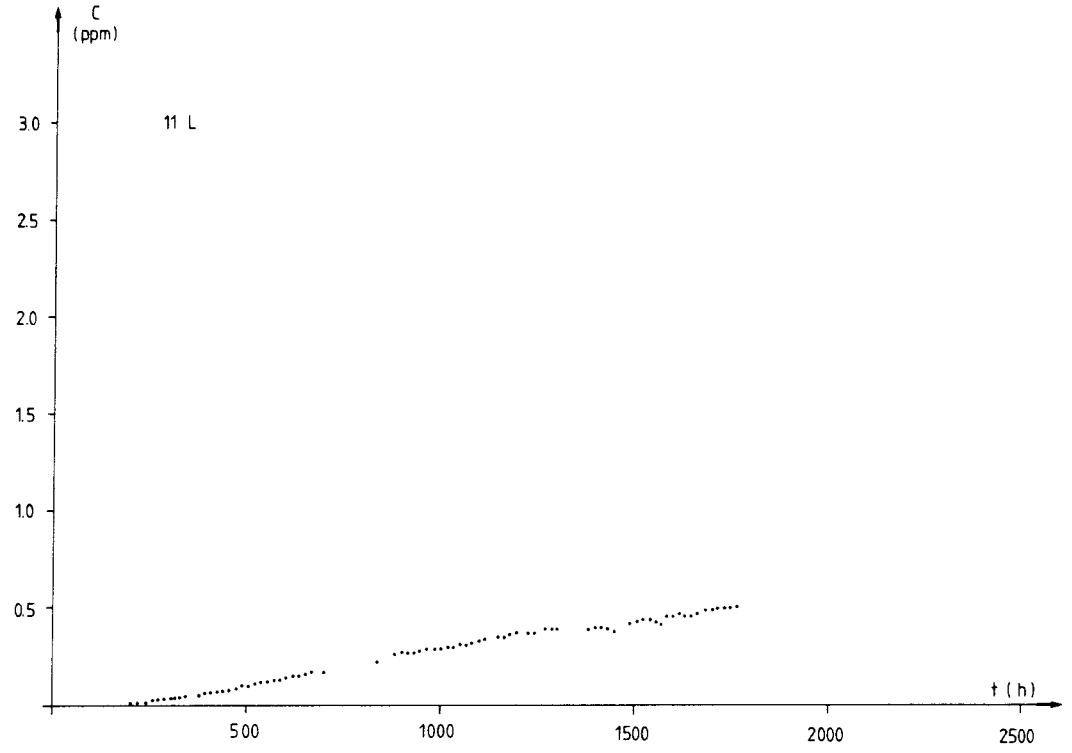

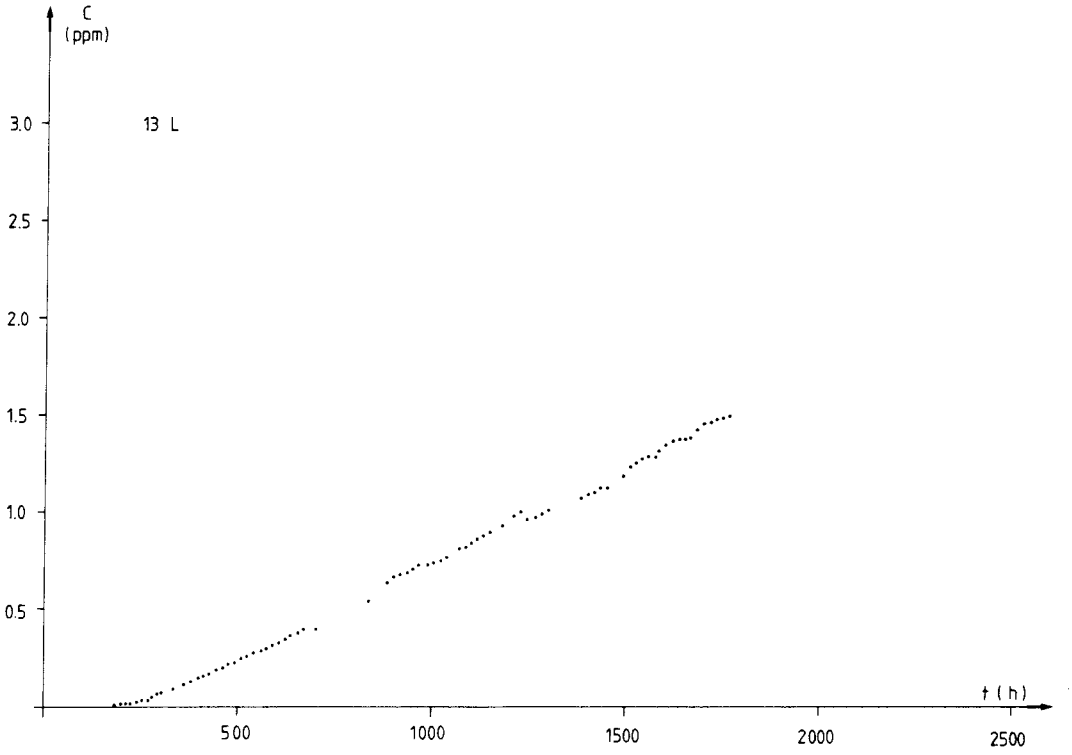

Fig 15b Breakthrough curves for Uranine in sections 11 L and 13 L.

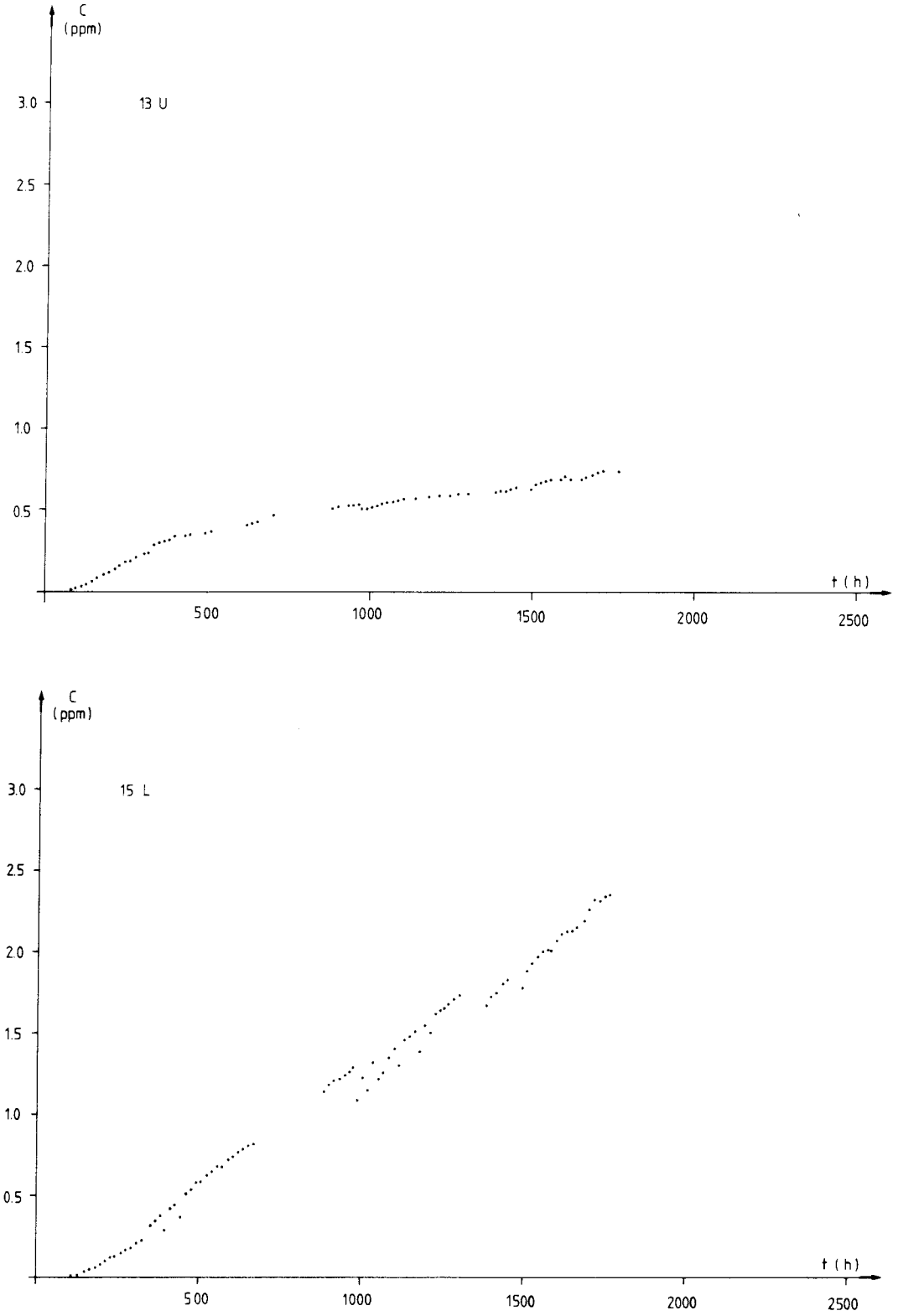

Fig 15c Breakthrough curves for Uranine in sections 13 U and 15 L.

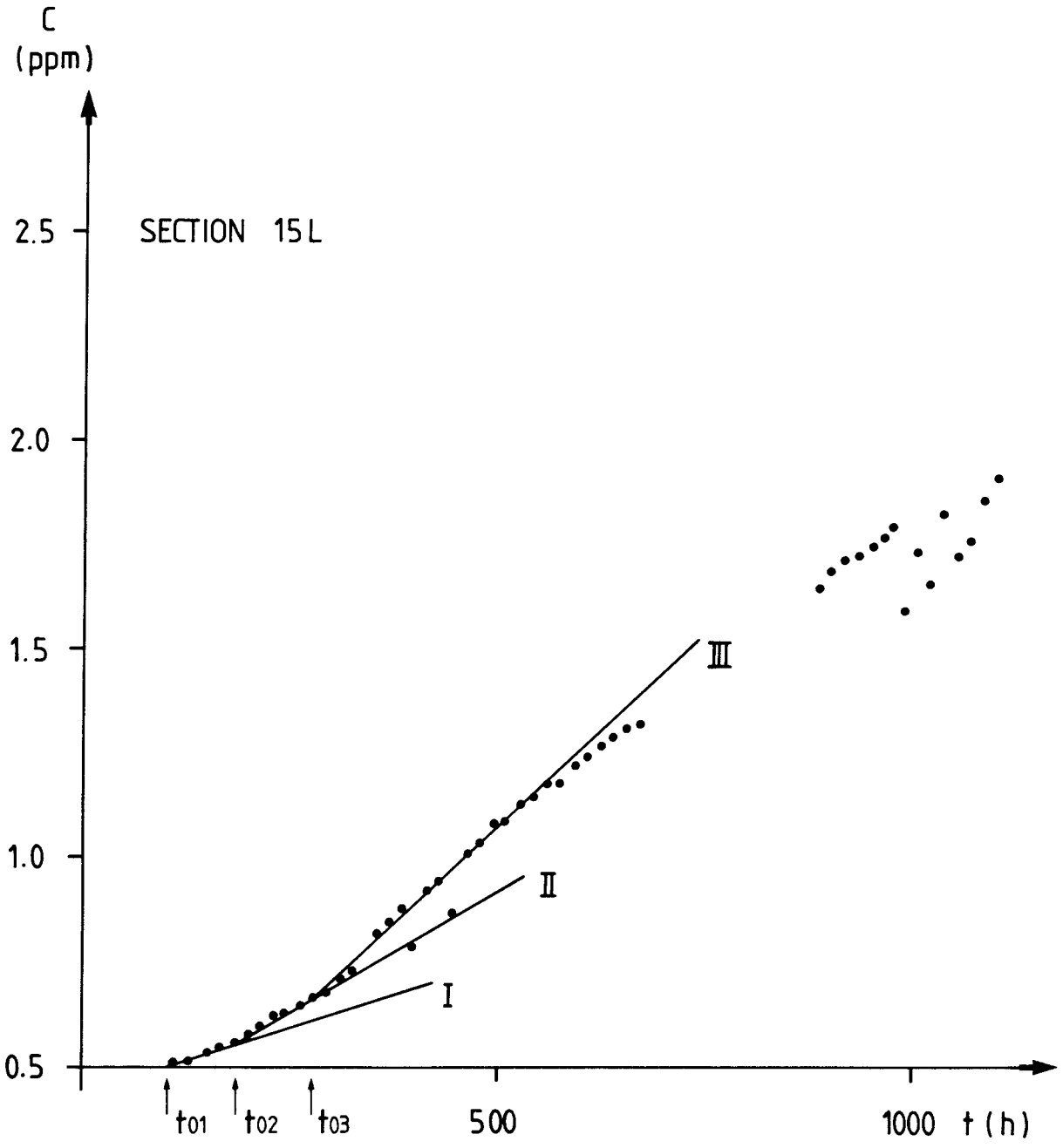

Fig 16 Breakthrough curve section 15 L showing the interpretation of the flow rate, q, and residence time, t_o.

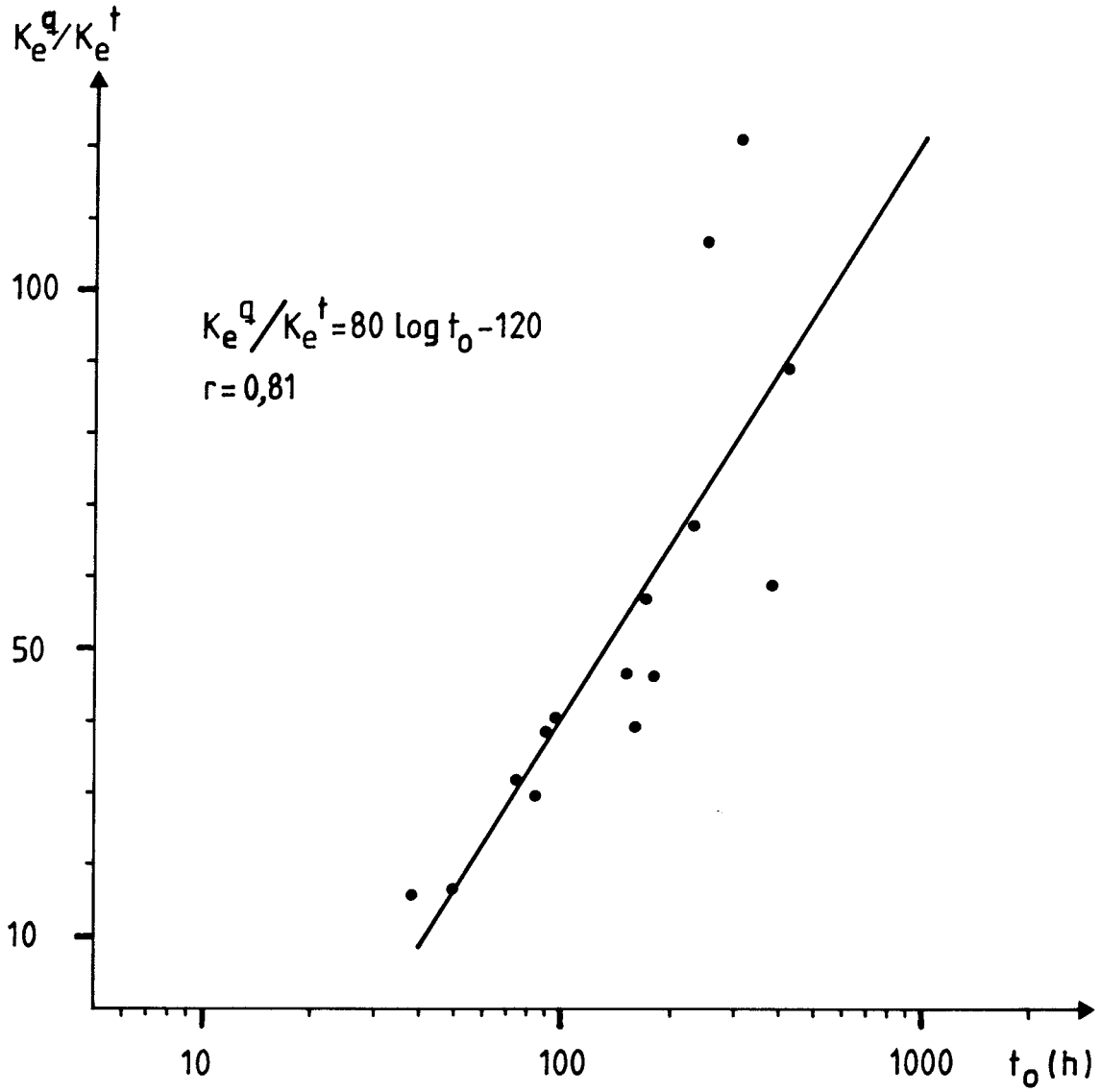

Fig 17 Hydraulic fracture conductivity ratio, K_e^q / K_e^t, versus the logarithm of residence time, t_o.

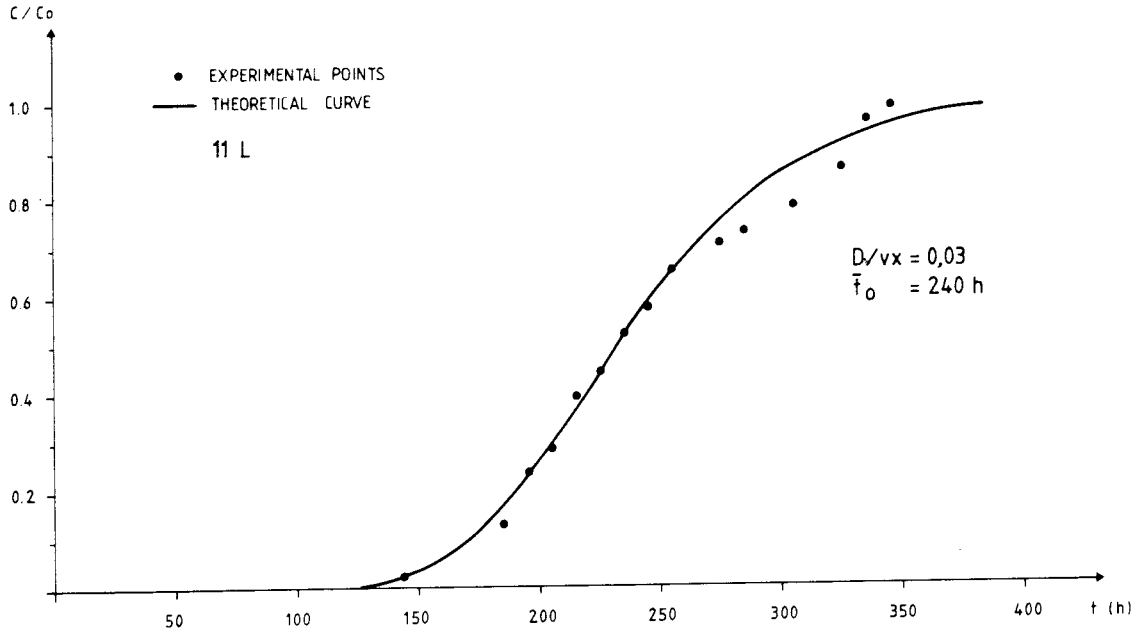

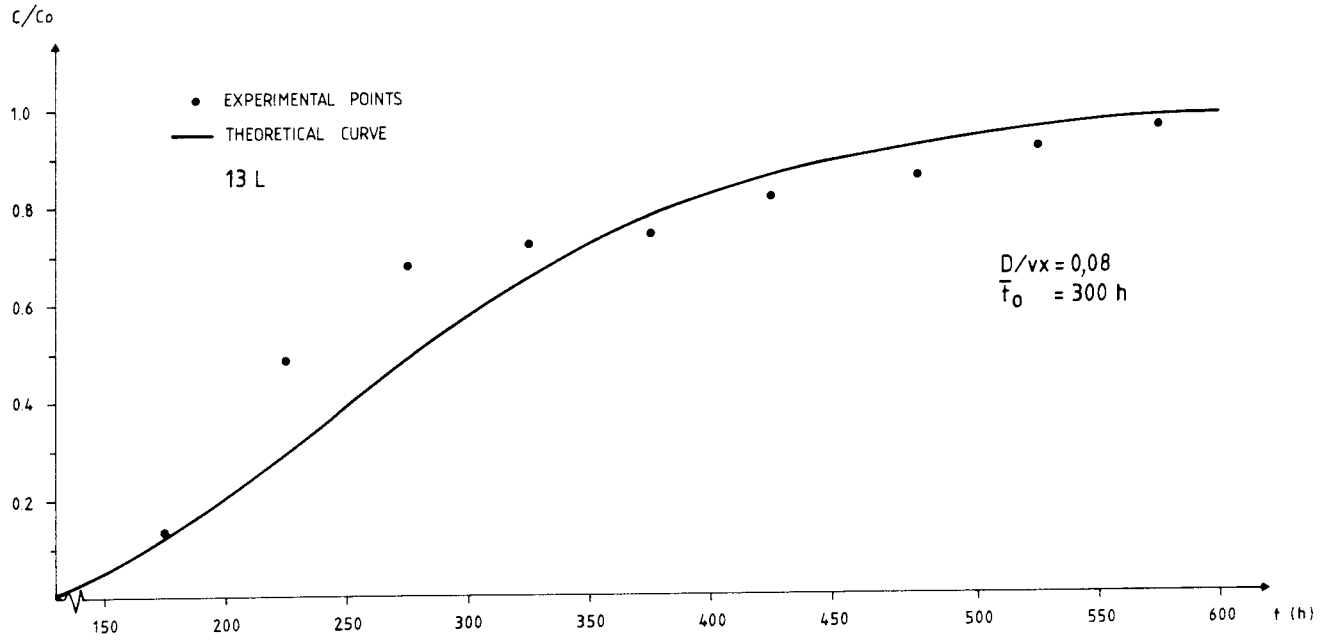

Fig 18a Experimental breakthrough curve for Uranine and fit with theoretical curves for sections 11 L and 13 L.

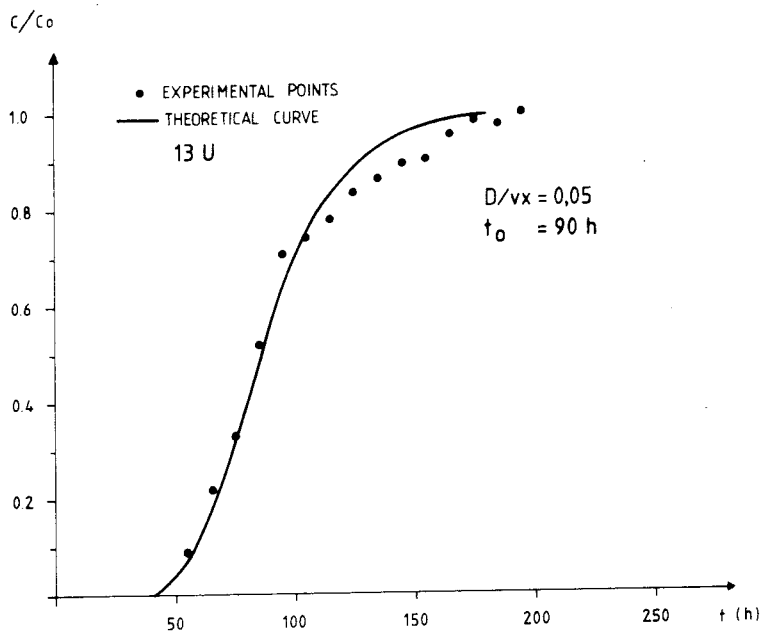

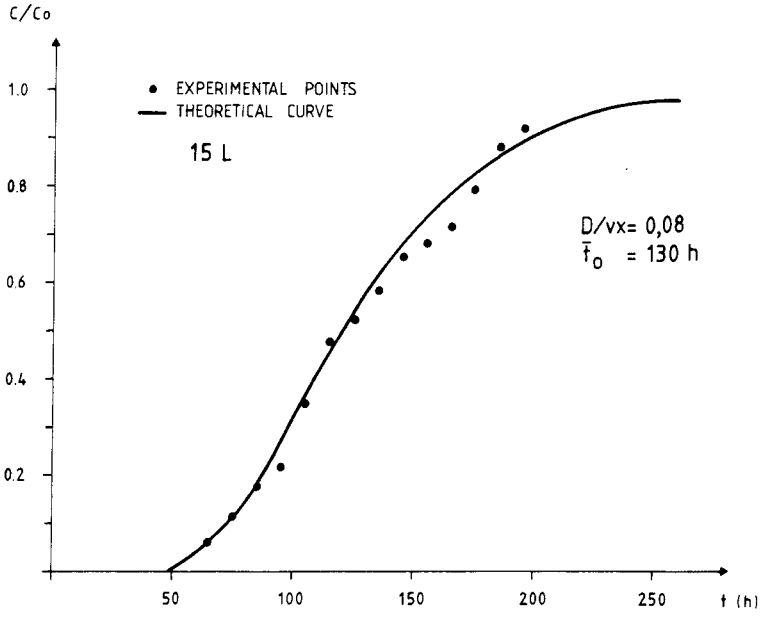

Fig 18b Experimental breakthrough curve for Uranine and fit with theoretical curves for sections 13 U and 15 L.

List of Technical Reports

1977–78
TR 121
KBS Technical Reports 1 – 120.
Summaries. Stockholm, May 1979.

1979
TR 79–28
The KBS Annual Report 1979.
KBS Technical Reports 79-01 – 79-27.
Summaries. Stockholm, March 1980.

1980
TR 80–26
The KBS Annual Report 1980.
KBS Technical Reports 80-01 – 80-25.
Summaries. Stockholm, March 1981.

1981
TR 81–17
The KBS Annual Report 1981.
KBS Technical Reports 81-01 – 81-16.
Summaries. Stockholm, April 1982.

1982
TR 82–28
The KBS Annual Report 1982.
KBS Technical Reports 82-01 – 82-27.
Summaries. Stockholm, July 1983.

1983
TR 83–77
The KBS Annual Report 1983.
KBS Technical Reports 83-01 – 83-76
Summaries. Stockholm, June 1984.

1984
TR 85–01
Annual Research and Development Report 1984
Including Summaries of Technical Reports Issued during 1984. (Technical Reports 84-01– 84-19)
Stockholm June 1985.

1985
TR 85–01
Annual Research and Development Report 1984
Including Summaries of Technical Reports Issued during 1984.
Stockholm June 1985.

TR 85–02
The Taavinunnanen gabbro massif. A compilation of results from geological, geophysical and hydrogeological investigations.
Bengt Gentzschein
Eva-Lena Tullborg
Swedish Geological Company
Uppsala, January 1985

TR 85–03
Porosities and diffusivities of some non-sorbing species in crystalline rocks.
Kristina Skagius
Ivars Neretnieks
The Royal Institute of Technology
Department of Chemical Engineering
Stockholm, 1985-02-07

TR 85–04
The chemical coherence of natural spent fuel at the Oklo nuclear reactors.
David B. Curtis
New Mexico, USA, March 1985

TR 85–05
Diffusivity measurements and electrical resistivity measurements in rock samples under mechanical stress.
Kristina Skagius
Ivars Neretnieks
The Royal Institute of Technology
Department of Chemical Engineering
Stockholm, 1985-04-15

TR 85-06
Mechanical properties of granitic rocks from Gideå, Sweden
Christer Ljunggren
Ove Stephansson
Ove Alm
Hossein Hakami
Ulf Mattila
Div of Rock Mechanics
University of Luleå
Luleå, Sweden, October 1985

TR 85-07
Complex forming properties of natural occurring fulvic acids
Part 1. Complexes with cadmium, copper and calcium
Jacob A. Marinsky,
A. Mathuthu,
M. Bicking and
J. Ephraim
State University of New York at Buffalo
Buffalo, New York 14214,
July 1985

TR 85-08

In situ one-year burial experiments with simulated nuclear waste glasses

Larry L Hench, Derek Spilman and T Buonaquisti
College of Engineering, Univ. of Florida, Gainesville, USA
Alexander Lodding
Chalmers Univ. of Technology, Gothenburg, Sweden
Lars Werme
SKB, Stockholm, Sweden

TR 85-09

Concentration and distribution of natural radionuclides at Klipperåsen and Bjulebo, Sweden

Björn Sundblad, Ove Landström, Rune Axelsson
Studsvik Energiteknik AB, Nyköping, Sweden

TR 85-10

Chemical interactions between the bentonite and the natural solutions from the granite near a repository for spent nuclear fuel

Bertrand Fritz and Marie Kam
Université Louis Pasteur de Strasbourg, Institut de Géologie, France
July 1985

TR 85-11

Hydrochemical investigations in crystalline bedrock in relation to existing hydraulic conditions: Experience from the SKB test-sites in Sweden

John Smellie, Nils-Åke Larsson
Swedish Geological Company, Uppsala, Sweden
Peter Wikberg
Royal Institute of Technology, Stockholm Sweden
Leif Carlsson
Swedish Geological Company, Göteborg, Sweden
November 1985